NASA TECHNICAL NOTE

NASA TN D-4691

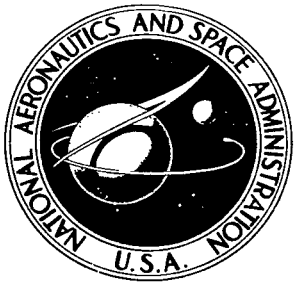

A QUASI-STEADY STATE ANALYSIS OF THE DYNAMIC BEHAVIOR OF A CONIC BODY MOVING IN A NONUNIFORM WAKE

by John DeFife and Theodore F. Hughes

Manned Spacecraft Center
Houston, Texas

NATIONAL AERONAUTICS AND SPACE ADMINISTRATION • WASHINGTON, D. C. • AUGUST 1968

A QUASI-STEADY STATE ANALYSIS OF THE DYNAMIC BEHAVIOR OF A CONIC BODY MOVING IN A NONUNIFORM WAKE

By John De Fife and Theodore F. Hughes

Manned Spacecraft Center
Houston, Texas

NATIONAL AERONAUTICS AND SPACE ADMINISTRATION

For sale by the Clearinghouse for Federal Scientific and Technical Information
Springfield, Virginia 22151 – CFSTI price $3.00

ABSTRACT

During reentry, the Apollo command module creates a wake of turbulent and reverse-flow conditions. When the earth-landing-system protective cover (forward heat shield) of the command module is jettisoned and moves within this wake, the kinetic energy of the cover is substantially reduced because of the reverse flows.

Equations were developed which allowed vectorial addition of wake velocities to those velocities of the forward heat shield. From these resultant vectors and from wind-tunnel aerodynamic data, forces and accelerations were calculated, and trajectories were generated which indicated that the reverse flows within the wake had a significant effect on the dynamic behavior of the protective cover and therefore caused recontact for low initial separation velocities.

CONTENTS

FIGURES

A QUASI-STEADY STATE ANALYSIS OF THE DYNAMIC BEHAVIOR OF A CONIC BODY MOVING IN A NONUNIFORM WAKE

By John De Fife and Theodore F. Hughes*
Manned Spacecraft Center

SUMMARY

A quasi-steady state analysis has been developed for predicting the dynamic behavior of a conic body set in motion in a turbulent wake. A series of static subsonic wind-tunnel tests was performed on scale models of the Apollo command module and the earth-landing-system protective cover (forward heat shield) of the command module. Included in the tests was a velocity and pressure survey conducted near and downstream of the command module which defined a large wake of turbulent and reverse-flow conditions. In addition, tests of two different forward heat-shield configurations were conducted within this wake to determine forces and moments and the effects of reverse flow. Equations were then developed which allowed vectorial addition of wake velocities to those velocities of the forward heat shield. From the resultant vectors and from wind-tunnel aerodynamic data, forces and accelerations were calculated, and trajectories were generated which indicated that the reverse flows within the wake have a significant effect on the dynamic behavior of the forward heat shield which causes recontact at low initial separation velocities. The forward heat-shield configuration used primarily on earth orbital missions (Block I) was found to require an initial instantaneous velocity greater than 50 ft/sec to avoid recontact. The lunar forward heat-shield configuration (Block II) was found to require an initial instantaneous velocity greater than 44 ft/sec to avoid recontact.

INTRODUCTION

One of the final phases of the Apollo mission is reentry into the atmosphere of the earth, which is followed by terminal descent using a parachute system. As the Apollo command module (CM) moves within the atmosphere at subsonic speeds, a wake is formed around and downstream of the CM trailing region.

The phenomenon of boundary-layer separation, associated with air flowing over the surface of a bluff body (such as the CM), causes a wake of turbulent conditions from the point of separation to the trailing region of the body. Beyond the point of

*ITT/Federal Electric Corporation.

separation, the air in the region near the CM surface flows in the direction opposite to the main stream flow. The boundary-layer separation and reverse-flow phenomena are described in detail in references 1 and 2. When the landing parachute protective cover, designated as the forward heat shield (FHS), is jettisoned and moves within the wake of the CM, the kinetic energy of the FHS is substantially reduced because of the reverse flows. Thus, to avoid recontact with the CM or to prevent fouling of the drogue parachutes, sufficient initial velocity of the FHS is required to overcome this energy loss. In addition, the initial velocity of the FHS must overcome the gravitational pull of the earth.

A series of static force and pressure tests in a subsonic wind tunnel was performed on scale models of two different FHS configurations in the wake of the CM. The aerodynamic characteristics of the FHS models were determined at a Mach number of 0.26 and at a Reynolds number of 2.37×10^6. The tests consisted of a wake survey and Block I and Block II static tests. The wake survey was a study of CM wake flow to determine the pressure gradients and the general flow pattern of the CM wake. The Block I static test was a study of the aerodynamic characteristics of the initial FHS configuration used primarily on earth orbital missions. The Block I test was conducted in the free stream and in the wake of the CM. The Block II static test was a repeat of Block I studies except that the lunar FHS configuration was tested and that an improved wind-tunnel testing technique was used.

For Block I, the wake disturbance caused by the FHS model support system was substantial. A technique was developed to compensate for the errors induced by the support system. Block II, with refined measuring equipment and different testing techniques, minimized strut interference effects. To compensate for the motionless test condition of the Block II FHS, special treatment was given to local wake velocity, local wake angle of attack, and instantaneous translational velocity of the FHS. An analytical method was devised to add these velocities vectorially, and the results led to true FHS flight conditions within the wake. Flight trajectories were then evaluated to show the effects of wake flow reversals acting on the FHS in motion.

SYMBOLS

The force vectors and angles presented in this paper are referenced about the body systems as shown in figure 1.

A_X FHS total acceleration in the X direction, ft/sec^2

A_Z FHS total acceleration in the Z direction, ft/sec^2

C_A FHS axial-force coefficient, $\frac{F_A}{q_\infty S}$

$C_{m, A}$ pitching-moment coefficient computed about theoretical apex of FHS, $\frac{M_A}{q_\infty SD}$

C_N FHS normal-force coefficient, $\frac{F_N}{q_\infty S}$

$C_{N, W}$ FHS normal-force coefficient in the wake

$C_{N, \infty}$ FHS normal-force coefficient in the free stream

D CM reference diameter, ft

D_X FHS displacement in the X direction relative to the CM, ft

D_Z FHS displacement in the Z direction relative to the CM, ft

F_A FHS axial force, lb

$F_{A, X}$ FHS axial-force component in the X direction, lb

$F_{A, Z}$ FHS axial-force component in the Z direction, lb

F_N FHS normal force, lb

$F_{N, X}$ FHS normal-force component in the X direction, lb

$F_{N, Z}$ FHS normal-force component in the Z direction, lb

I_{FHS} FHS pitching moment of inertia about the center of gravity (c. g.), slug-ft^2

M_A pitching moment computed about the theoretical apex of the FHS, ft-lb

$M_{c. g.}$ pitching moment computed about the center of gravity of the FHS, ft-lb

m FHS mass, slugs

q_t total wake dynamic pressure, lb/ft^2

q_w local wake dynamic pressure, lb/ft^2

q_∞ free-stream dynamic pressure, lb/ft^2

S CM reference area, $\frac{\pi D^2}{4}$, ft^2

t time, sec

V_{FHS} FHS translational velocity relative to the CM, ft/sec

V_t FHS total velocity relative to the air in the wake, ft/sec

$V_{t, X}$ component of the FHS total velocity relative to the wake (in the X direction), ft/sec

$V_{t, Z}$ component of the FHS total velocity relative to the wake (in the Z direction), ft/sec

V_W local wake velocity relative to the CM, ft/sec

$V_{W, X}$ component of local wake velocity relative to the CM (in the X direction), ft/sec

$V_{W, Z}$ component of local wake velocity relative to the CM (in the Z direction), ft/sec

V_X FHS translational velocity relative to the CM (in the X direction), ft/sec

V_Z FHS translational velocity relative to the CM (in the Z direction), ft/sec

V_∞ free-stream velocity, ft/sec

W FHS weight, lb

W_X FHS weight component in the X direction, lb

W_Z FHS weight component in the Z direction, lb

X wind axes parallel to free-stream velocity

X/D wind-tunnel coordinate position of the FHS in the X direction

x_A FHS theoretical apex location in CM reference system at t = 0, ft

$x_{c.g.}$ FHS center-of-gravity location in CM reference system at t = 0, ft

Z wind axes perpendicular to the free-stream velocity

Z/D wind-tunnel coordinate position of the FHS in the Z direction

z_A FHS theoretical apex location in CM reference system at t = 0, ft

$z_{c.g.}$ FHS center-of-gravity location in CM reference system at t = 0, ft

α_{CM} angular position of the CM relative to the free-stream velocity, deg

α_{FHS} angular position of FHS relative to the free-stream velocity vector, deg

α_t total angle of attack of the FHS relative to the air in the wake, ft/sec

α_W local wake angle of attack relative to the free-stream velocity vector, deg

$\dot{\alpha}_{FHS}$ angular velocity of the FHS, rad/sec

$\ddot{\alpha}_{FHS}$ angular acceleration of the FHS, rad/sec^2

Γ_{FHS} FHS flight-path angle relative to the CM, deg

Γ_∞ CM flight-path angle relative to local vertical, deg

ΔC_A FHS axial-force coefficient errors induced by strut

$\Delta C_{m,A}$ pitching-moment coefficient computed about the theoretical apex of FHS errors induced by the strut

ΔC_N FHS normal-force coefficient errors induced by strut

$\Delta\alpha$ correction applied to the angular position of the FHS because of the translational velocity of the FHS, deg

ρ_W wake density, $slug/ft^3$

ρ_∞ free-stream density, $slug/ft^3$

MODELS AND TESTING TECHNIQUES

All tests (the wake survey, the Block I static test and the Block II static test) were conducted in a subsonic, 7.75- by 11-foot, continuous-flow, closed-circuit, single-return-type wind tunnel. Test conditions were set at a Mach number of 0.26 and at a Reynolds number of 2.37×10^6. These conditions were considered to be satisfactory since the test conditions were past the transition Reynolds number region and were similar to previous Apollo wind-tunnel tests which had shown very small changes in aerodynamic characteristics as a function of Reynolds number.

The CM model used in the tests was built to a scale of 0.10. The model was constructed of wood, steel, and aluminum with a simulated egress tunnel, parachute packs, and drogue mortars. The model orientation relative to the wind-tunnel free stream and to the FHS models is shown by figure 1. The Block I and Block II FHS models were machined aluminum with holes drilled for mounting purposes. The primary differences in Block I and Block II FHS configurations, and also the general shape and pertinent components of the CM, are shown in figure 2.

Wake Survey

The CM was held rigid in the center of the tunnel by horizontal support rods at an angle of attack of 170° with 0° sideslip. Testing was conducted at a constant dynamic pressure of approximately 100 psf. Figure 3 shows the wind tunnel, the CM, the horizontal support rods, and the pressure measuring apparatus (pressure rake). The pressure rake was constructed of horizontal and vertical aluminum slides which held a vertical bar to which 31 pitot tubes were attached. The unit could be moved horizontally, vertically, and downstream. Each pitot tube had individual limp tufts which were used as flow-direction indicators. The pitot tubes were oriented in the free-stream direction only and, therefore, were incapable of measuring pressures accurately in any other direction. Pressures were measured at various positions downstream and in the wake of the CM. The tufts described the general size and shape of the wake.

Block I Static Test

Figures 4(a) and 4(b) show typical installations in which forces and moments on the FHS were measured in the free stream. As shown in the figure, the model was held rigid at different angles of attack by a horizontal strut. Figures 4(c), 4(d), and 4(e) show installations in which the FHS was tested downstream in the wake of the CM. The CM was mounted on vertical support rods and was fixed at a constant angle of attack of 170°. By a series of holes drilled through plates mounted on the floor and ceiling and by drilled flanges attached to the ends of the vertical support rod, the CM could be positioned at various distances upstream and off-center in either direction from the FHS. The end of the horizontal strut attached to the FHS had a ball joint which allowed some variation in the angle of attack. This ball joint, together with the capability of reclamping the FHS on the strut at different positions, allowed testing at

angles of attack from 125° to 230°. Forces and moments on the FHS were measured by a strain-gage balance system and were converted to aerodynamic coefficients.

Block II Static Test

The Block II FHS differed from the Block I FHS because of the simulated escape-tower leg wells which were incorporated and because of a cutout for the reaction control engine. In addition, the Block II FHS did not have an upper cone portion (fig. 2). The Block II model was held rigid in the center of the wind tunnel by a vertical support strut attached to a load-measuring apparatus beneath the floor. The strut was surrounded by sheet steel which had been rolled into a streamlined shape and attached to the floor (independent of the strut). The FHS model could be rotated from 0° to 360° (fig. 5). This type of model support was used to minimize strut effects and to reduce errors incurred from data scatter.

Since the CM was held at a pitch of 0° in relation to the wind tunnel, the pattern of the wake was nearly symmetrical about the FHS horizontal center line. Because of the symmetry, a dummy strut and a "wind shield" identical to the floor-mounted shield were also attached to the top of the FHS model and to the ceiling (fig. 5(a)). This image technique induced the same disturbance above and below the FHS model. An extrapolation can then be made to determine the effects of one support, or if required, of no support. This system of determining model-support effects is discussed in reference 3. The three primary tests performed were as follows:

1. The FHS in free stream
2. The FHS in the wake of the CM with one support strut
3. The FHS in the wake of the CM with a mirror-image strut

TESTS RESULTS

Wake Survey

Figure 3(b) shows the system in an actual test in which the flow indicators (tufts) attached to the pitot tubes describe the velocity patterns of the wake and confirm the reverse flow. Because of the large variation in angularity and since the pressure rake could be oriented only in the free-stream direction, the pressure measurements were considered to be invalid. A group of photographs of the pressure rake, with tufts at various positions downstream of the CM, illustrated the size and shape of the wake. Figure 6 was constructed from these photographs. Although free of the FHS disturbance, the flow pattern was used to support evaluations of Block I and Block II tests and analyses.

Block I Static Test

Aerodynamic characteristics determined from static tests of the Block I FHS in the free stream are presented in figure 7. Similar data for the FHS in the wake of the CM are presented in figure 8 which shows axial and normal aerodynamic coefficients plotted against angles of attack from approximately 125° to 230°. Data for this figure were gathered with the FHS downstream and in the wake of the CM at a coordinate of X/D = 1.0 and Z/D = 0.3. It is important to note the scatter of data points on the plot in figure 8. Scatter of the data in figure 8 is attributed to wake disturbance and strut effects. Figure 7 is similar to figure 8, except that forces and moments were measured with the CM removed from the tunnel. Again, the scatter of the data is attributed primarily to FHS strut effects. Data from the wind-tunnel tests are plotted in figures 7 and 8 and are representative of scatter for all 21 coordinate points of data reduction. The faired data of figure 9 lie in a path between the extremes of the data scatter indicated by the fairings shown in figure 8.

Block II Static Test

Figure 10 represents aerodynamic characteristics of the Block II FHS supported by an image strut system with forces and moments measured in the free stream. By using streamlined struts, repeatability was improved by approximately 75 percent. The curves in figure 11 are similar to the curves in figure 10, but forces and moments were measured in the wake of the CM at a coordinate position of X/D = 0.76, and Z/D = 0. Figures 10 and 11 compare the single- and double-strut data. From a limited number of double-strut tests used in conjunction with test data from all coordinate positions throughout the wake, the no-support condition was determined by using the image method presented in reference 3. Figure 12 shows faired curves for the FHS supported by a single strut at various positions downstream of the CM and in the free stream.

METHOD OF ANALYSIS

Block I and Block II Static Tests

Block I and Block II analyses are combined in this section because they are identical except for the special treatment given to the respective strut effects and because of the special treatment given to angles of attack and dynamic pressure in the Block II studies. The method of analysis and the difference of treatise are explained in the following paragraphs.

Forces and moments on the FHS were measured by a strain-gage balance system and were converted to aerodynamic coefficients. After assembling all of the data for each study, computer programs were written to solve mathematical equations which ultimately yielded trajectories of the FHS for various initial velocities. From these trajectories, the instantaneous initial velocity required to avoid recontact was determined. Force vectors and moments relative to testing models along with general reference dimensions are shown in figure 1. Force and moment equations as a

function of aerodynamic coefficient, dynamic pressure, CM diameter, and CM area were written in FORTRAN language for use in the computer program. These equations and the solutions leading to the accelerations are

$$F_A = C_A \left(q_\infty S\right) \tag{1}$$

$$F_N = C_N \left(q_\infty S\right) \tag{2}$$

and

$$M_A = C_{m,A} \left(q_\infty SD\right) \tag{3}$$

The moment about the center of gravity of the FHS may be found by the following equation.

$$M_{c.g.} = M_A + F_A \left(z_{c.g.} - z_A\right) - F_N \left(x_{c.g.} - x_A\right) \tag{4}$$

Components of the normal and axial forces in the X and Z directions acting on the FHS at any angle of attack, as shown by figure 13, are computed from

$$F_{A,X} = F_A \cos \left(\alpha_{FHS}\right) \tag{5}$$

$$F_{A,Z} = -F_A \sin \left(\alpha_{FHS}\right) \tag{6}$$

$$F_{N,X} = F_N \sin \left(\alpha_{FHS}\right) \tag{7}$$

$$F_{N,Z} = F_N \cos \left(\alpha_{FHS}\right) \tag{8}$$

By using the FHS weight and the CM flight-path angle, components of the weight in the X- and Z-axis systems are computed by

$$W_X = W \cos \left(\Gamma_\infty\right) \tag{9}$$

and

$$W_Z = W \sin \left(\Gamma_\infty\right) \tag{10}$$

With the components and relationships computed from equations (1) to (10), values of acceleration in X and Z directions are computed from

$$A_X = \frac{F_{A,X} + F_{N,X} - W_X}{m} \tag{11}$$

$$A_Z = \frac{F_{N,Z} + F_{A,Z} - W_Z}{m} \tag{12}$$

The angular acceleration is given by

$$\ddot{\alpha}_{FHS} = \frac{M_{c.g.}}{I_{FHS}} \tag{13}$$

Figure 14 indicates the related velocities and angles.

The accelerations A_X, A_Z, and $\ddot{\alpha}_{FHS}$ were integrated by a digital computer; and solutions of velocities, distances, and angular displacements of the FHS were determined. The integrations are

$$V_X = \int A_X \cdot dt + \left(V_X\right)_{t=0} \tag{14}$$

$$V_Z = \int A_Z \cdot dt + \left(V_Z\right)_{t=0} \tag{15}$$

$$\dot{\alpha}_{FHS} = \int \ddot{\alpha}_{FHS} \cdot dt + \left(\dot{\alpha}_{FHS}\right)_{t=0} \tag{16}$$

$$D_X = \int V_X \cdot dt + \left(D_X\right)_{t=0} \tag{17}$$

$$D_Z = \int V_Z \cdot dt + \left(D_Z\right)_{t=0} \tag{18}$$

$$\alpha_{FHS} = \int \dot{\alpha}_{FHS} \cdot dt + \left(\alpha_{FHS}\right)_{t=0} \tag{19}$$

From these solutions, trajectories of the FHS were plotted for Block I and Block II as shown in figures 15 and 16, respectively. These plots describe flight paths and can be used to predict recontact or separation for various initial instantaneous velocities. The trajectories with velocities going through zero in the X direction indicate potential recontact or drogue parachute fouling.

To compensate for strut effects on the wakes of Block I and Block II, special treatment was given to equations (1), (2), and (3); and the effects of this treatment are reflected throughout the mathematical analysis. From equations

$$F_A = C_A\left(q_\infty S\right) \tag{1}$$

$$F_N = C_N\left(q_\infty S\right) \tag{2}$$

$$M_A = C_{m,A}\left(q_\infty SD\right) \tag{3}$$

substitute

$$C_A = C_A \pm \Delta C_A$$

$$C_N = C_N \pm \Delta C_N$$

and

$$C_{m,A} = C_{m,A} \pm \Delta C_{m,A}$$

into equations (1), (2), and (3), thus

$$F_A = \left(C_A \pm \Delta C_A\right) \cdot \left(q_\infty S\right) \tag{20}$$

$$F_N = \left(C_N \pm \Delta C_N\right) \cdot \left(q_\infty S\right) \tag{21}$$

and

$$M_A = \left(C_{m,A} \pm \Delta C_{m,A}\right) \cdot \left(q_\infty SD\right) \tag{22}$$

The values used in the Block I analysis were $\Delta C_A = \pm 0.01$, $\Delta C_N = \pm 0.01$, and $\Delta C_{m,A} = \pm 0.01$. Forces and moments were calculated for any given angle of attack; whether influenced by a negative, a positive, or a neutral increment. In addition, the computer interpolated for aerodynamic coefficients between load-measuring points of the coordinate system to determine influence of the coefficients on the FHS. To determine the minimum initial velocity required, the most restrictive combination of Δ coefficients was used.

In Block II, the strut effects were minimized by streamlined supports. The supports included one strut and the mirror-image strut. An extrapolation was made for the no-strut condition, which proved to be the most restrictive case.

To compensate for the motionless test condition of the FHS in the wake, special treatment was given to the local wake velocity, the local wake angle of attack, and the instantaneous translational velocity of the FHS. Equations involving these velocities and angles were added vectorially, and the results led to true FHS flight conditions within the wake.

For the derivation of these equations, two important assumptions were made: (1) that the air density of the wake ρ_W was equal to the air density of the free stream ρ_∞ and (2) that the flow field immediately adjacent to the FHS was uniform.

Figure 14 indicates a velocity diagram of the FHS acting within the wake and is a pictorial description of the equations of motion. The derivations of the equations of motion are

$$\frac{V_W}{V_\infty} = \sqrt{\frac{q_W}{q_\infty}} \tag{23}$$

$$V_{FHS} = \sqrt{V_X^2 + V_Z^2} \tag{24}$$

$$\Gamma_{FHS} = \tan^{-1} \frac{V_Z}{-V_X} \tag{25}$$

$$V_{W,X} = -V_W \cdot \cos \alpha_W \tag{26}$$

$$V_{W,Z} = V_W \cdot \sin \alpha_W \tag{27}$$

$$V_{t,X} = V_X + V_{W,X} \tag{28}$$

$$V_{t,Z} = V_Z + V_{W,Z} \tag{29}$$

$$V_t = \sqrt{V_{t,X}^2 + V_{t,Z}^2} \tag{30}$$

$$\alpha_t = \tan^{-1} \frac{V_{t,Z}}{-V_{t,X}} \tag{31}$$

$$q_t = 1/2 \rho_\infty V_t^2 \tag{32}$$

$$\Delta\alpha = \alpha_t - \alpha_W \tag{33}$$

In the computer program, all aerodynamic coefficients were assumed to be functions of $\alpha_{FHS} - \Delta\alpha$.

Before these equations can be solved, two unknowns must be determined for most coordinate positions: the wake angle of attack and the wake pressure. An analogous condition exists between the free-stream tests and the wake tests which allows an approximate solution for these unknowns. If, for example, a normal force of zero were measured on the FHS at a particular angle of attack in the free stream, then a corresponding zero force measured at any given coordinate position within the wake must result from the same angle of attack as the free stream. Therefore, the wake

angle of attack is readily solved for all coordinate positions except those immediately adjacent to the CM. At these positions, the most radically turbulent regions of the wake exist. For this reason, and because the FHS is in this region for only a short period of time, angles of attack and wake dynamic pressure were not determined.

Figure 17 is an arbitrary-wake aerodynamic plot, compared to a corresponding free-stream aerodynamic plot and adjusted to such a position that the curves have similar shapes. The zero normal-force coefficient of the free stream at an angle of attack of 360° coincides with the zero normal-force coefficient at 190° of the wake plot. Therefore, the wake angle of attack is 190°. This method was used for most of the coordinate positions in the wake of Block II.

The wake dynamic pressure was determined by the ratios of coefficients at the corresponding maximum and minimum points of both curves in figure 17, thus a general solution is

$$F = C_{N,\infty}\, S q_W = C_{N,W}\, q_\infty\, S \tag{34}$$

$$\frac{C_{N,\infty}}{C_{N,W}} = \frac{q_\infty}{q_W} \tag{35}$$

$$F_N = \left(C_N \pm \Delta C_N\right)\left(\frac{q_\infty}{q_W}\right)\left(q_t\right)\, S \tag{36}$$

similarly

$$F_A = \left(C_A \pm \Delta C_A\right)\left(\frac{q_\infty}{q_W}\right)\left(q_t\right)\, S \tag{37}$$

$$M_A = \left(C_{m,A} \pm \Delta C_{m,A}\right)\left(\frac{q_\infty}{q_W}\right)\left(q_t\right)\, SD \tag{38}$$

Equations (36), (37), and (38) lead to accelerations, velocities, distances, and angular displacements for plotting the Block II FHS trajectories.

To determine the effects of various assumptions made in this study, comparison trajectories were generated. The addition of the wake angle of attack and the dynamic pressure calculations to the basic simulation resulted in an increase of 2 ft/sec in the initial velocity required.

Also, calculations were made to determine the effects of neglecting pitch damping. The values of damping coefficient used in this comparison were ± 0.02. The resulting change in the velocity required was less than ± 1 ft/sec.

The basic assumption of a quasi-steady state analysis was verified by the calculation of the reduced-frequency parameter. A value of 4 cps was calculated at a wake position of $X/D = 0.5$, $Z/D = 0$.

Results of Analysis

The results of the wind-tunnel tests combined with the mathematical analysis are as described in the following paragraphs.

1. Wake survey analysis — The wake flow pattern was determined by limp tufts (which describe reverse flow), vortices, and eddy currents. An approximation of the wake is shown in figure 6.

2. Block I static analysis — Solved equations of motion depicting the flight trajectories of the Block I FHS in the wake of the CM indicated that a minimum initial instantaneous velocity greater than 50 ft/sec is required for complete separation. The flight trajectory is depicted in figure 15.

3. Block II static analysis — The minimum initial instantaneous velocity of the Block II FHS for complete separation was found to be greater than 44 ft/sec. Figure 16 describes the flight trajectory.

CONCLUDING REMARKS

A quasi-steady state analysis has been developed for predicting the dynamic behavior of a conic body set in motion in an incompressible fluid of turbulent and reverse flow conditions.

The phenomenon of boundary-layer separation associated with air flowing over a bluff body causes a wake of turbulent and reverse-flow conditions from the point of separation to the trailing region of the body. The Apollo command module, a bluff body, creates such conditions during reentry. When the forward heat shield of the command module is jettisoned and moves within the wake, the kinetic energy of the forward heat shield is substantially reduced because of the reverse flows caused by the command module. Therefore, to avoid recontact, sufficient initial velocity of the forward heat shield is required to overcome this energy loss.

Static wind-tunnel tests were performed on scale models to determine forces and moments acting on the forward heat shield in the wake of the command module. A computer program was written to solve equations involving these forces and moments and ultimately yielded trajectories of the forward heat shield for various initial velocities. Using these trajectories, the minimum initial velocities required to avoid recontact were determined. Results of the tests and analysis were as follows.

1. A large wake of turbulent and reverse-flow conditions was defined near and downstream of the trailing region of the command module.

2. The turbulent and reverse-flow region of the command module wake caused recontact of the forward heat shield for low initial separation velocities following jettisoning of the forward heat shield.

3. The minimum initial instantaneous velocities of the two different forward heat-shield configurations tested were found to be greater than 44 ft/sec for the Block II forward heat shield and greater than 50 ft/sec for the Block I forward heat shield.

Manned Spacecraft Center
National Aeronautics and Space Administration
Houston, Texas, March 29, 1968
914-50-10-09-72

REFERENCES

1. Dwinnell, James H.: Principles of Aerodynamics. McGraw-Hill Book Company, Inc., 1949, pp. 160, 161, 162, and 163.

2. Kreith, Frank: Principles of Heat Transfer. International Textbook Company, 1958, pp. 366 and 367.

3. Pope, Alan Y.: Wind-Tunnel Testing. Second ed., John Wiley & Sons, Inc., 1954, p. 156.

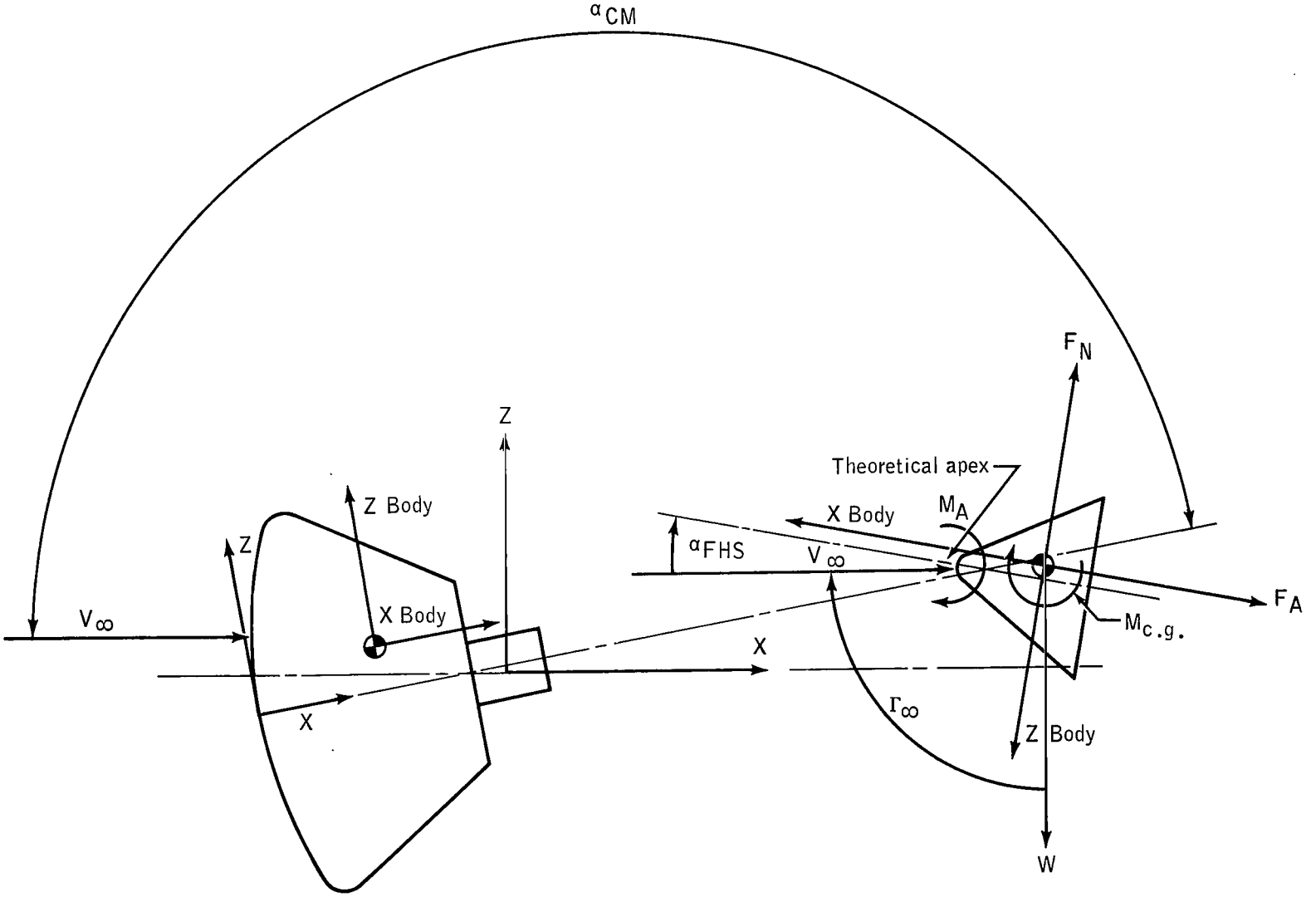

Figure 1. - Schematic of the forward heat shield (FHS) in the wake of the command module (CM) showing force vectors and angles.

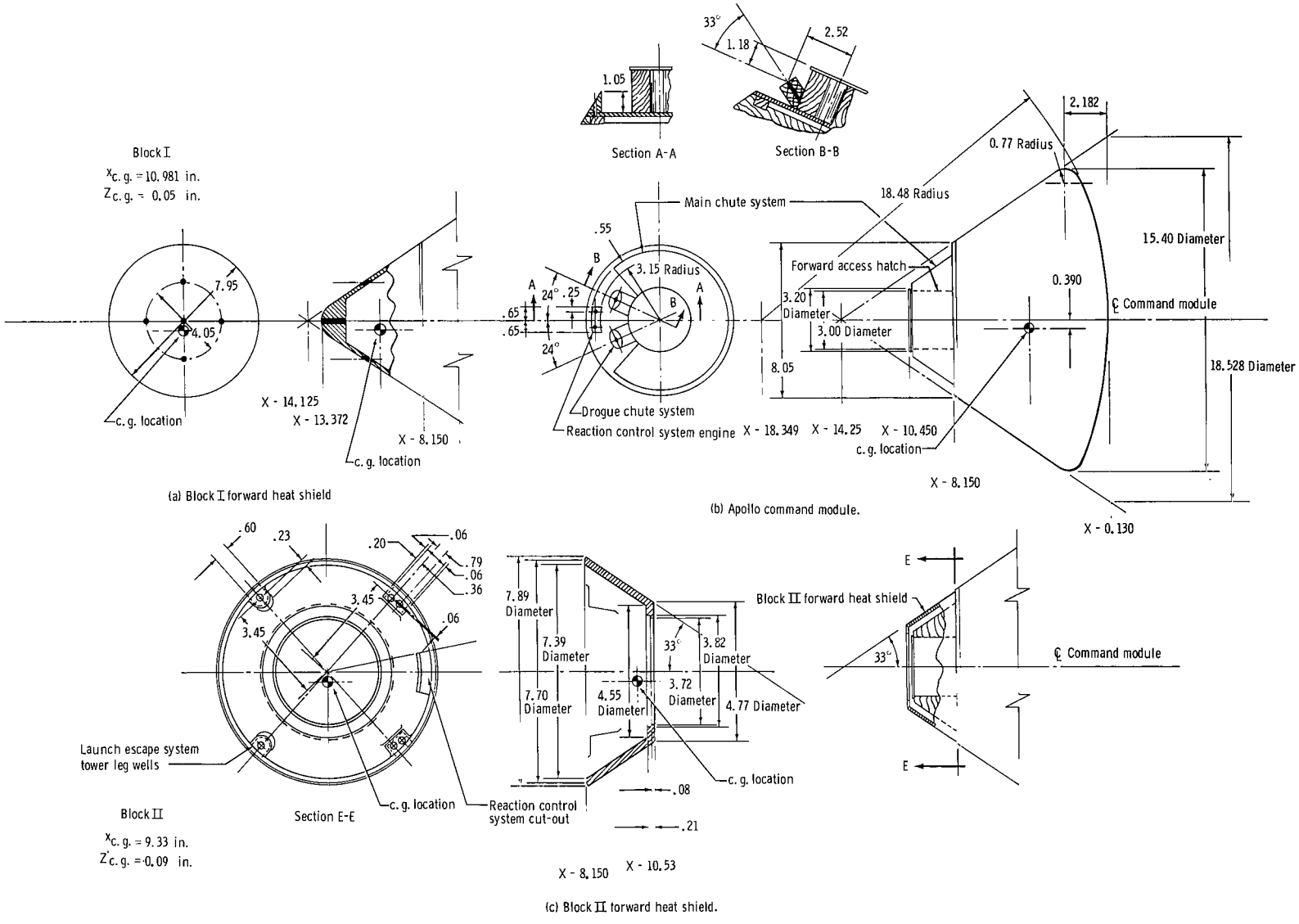

Figure 2. - Detail drawing of the Apollo command module and the Block I and Block II forward heat shields, 0.10-scale models, with all dimensions in inches.

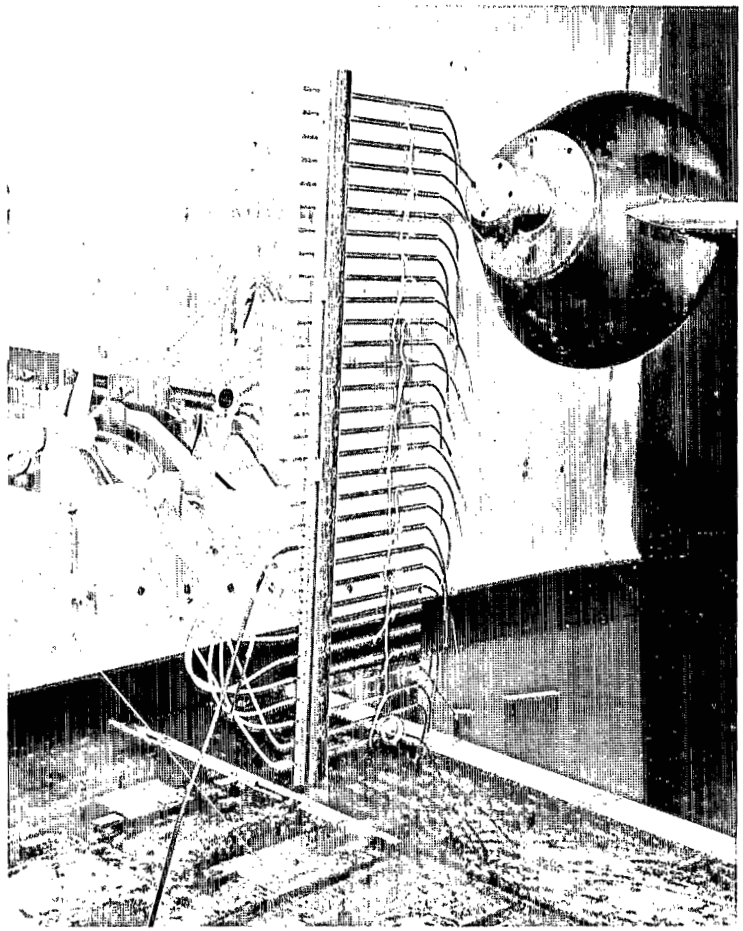

(a) Command module and pressure measuring apparatus.

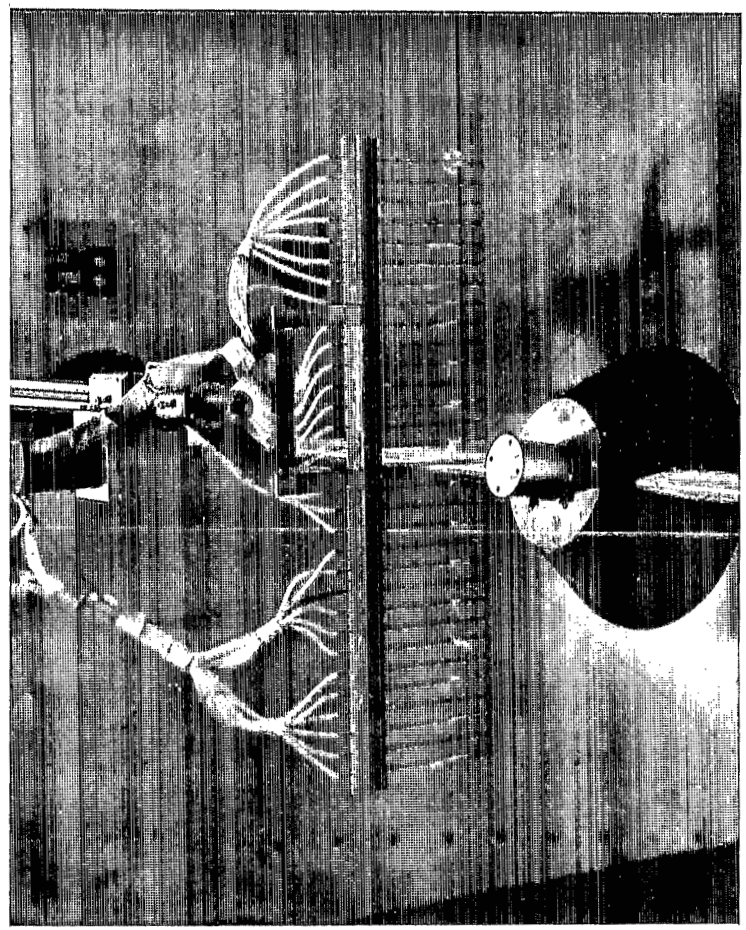

(b) Command module, pressure measuring apparatus, and limp tufts in actual test.

Figure 3. - Wind-tunnel installation photographs.

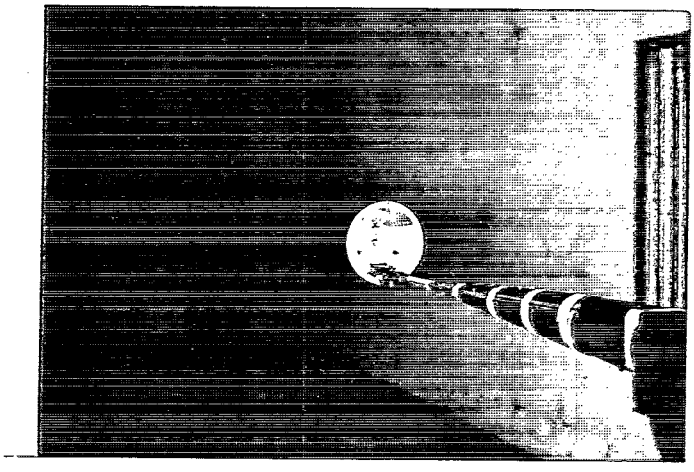

(a) Forward heat shield held by horizontal strut in free-stream test.

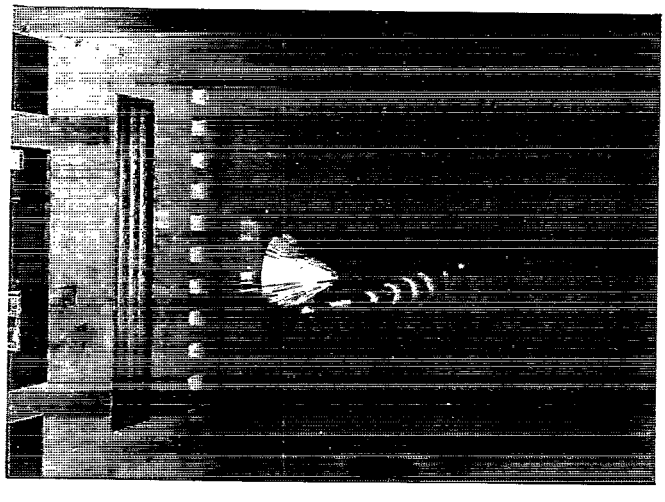

(b) Forward heat shield held by horizontal strut at angle of attack of 90°.

Figure 4. - Wind-tunnel installation photographs of the Block I forward heat-shield test.

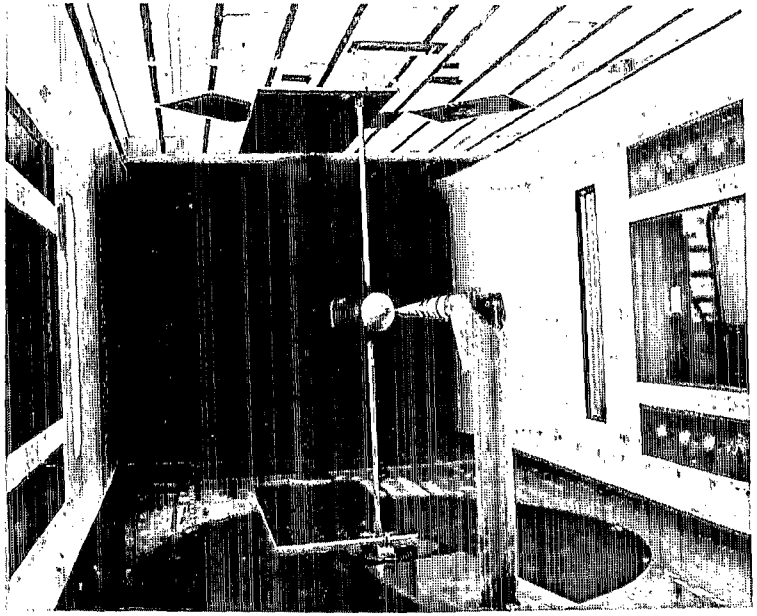

(c) Forward heat shield in wake of command module.

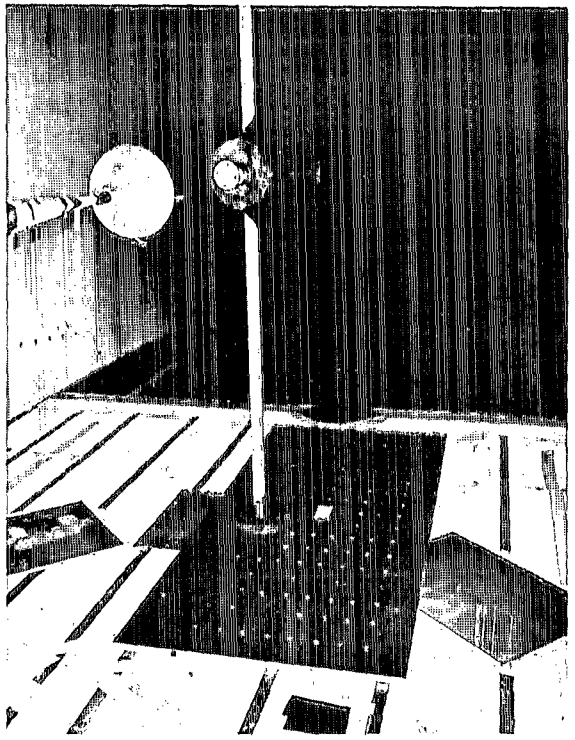

(d) Forward heat shield approximately 5 feet downstream (full scale) from command module.

Figure 4. - Continued.

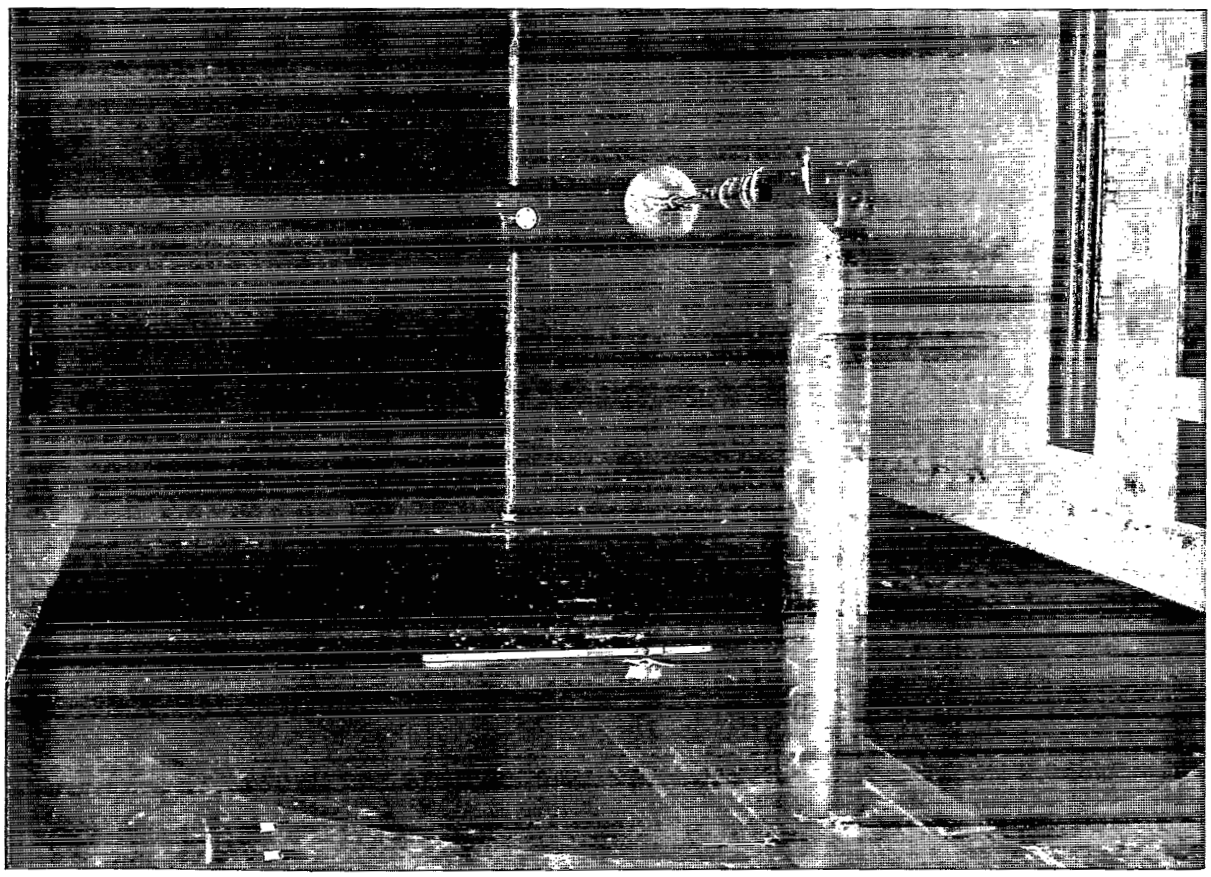

(e) Forward heat shield approximately 20 feet (full scale) downstream from command module.

Figure 4. - Concluded.

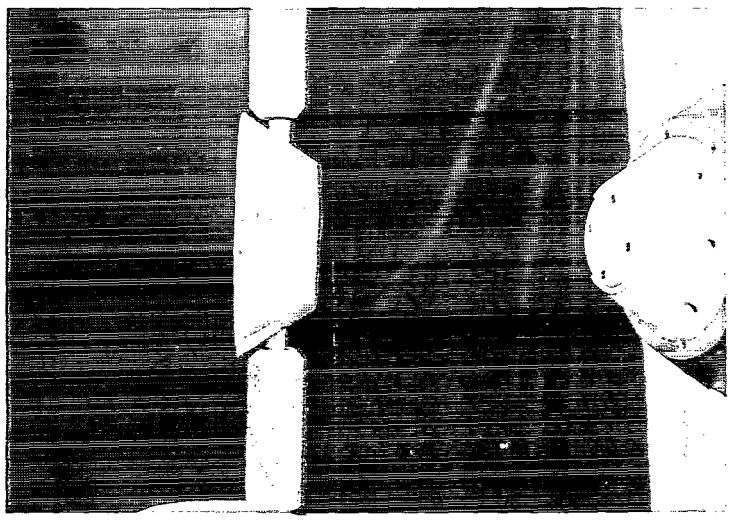

(a) Forward heat-shield configuration.

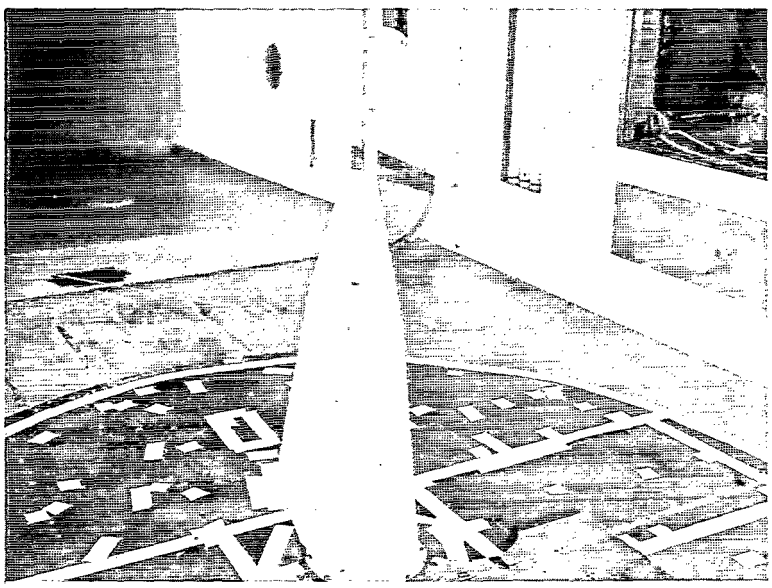

(b) Forward heat-shield free-stream test.

Figure 5. - Wind-tunnel installation photographs of the Block II test.

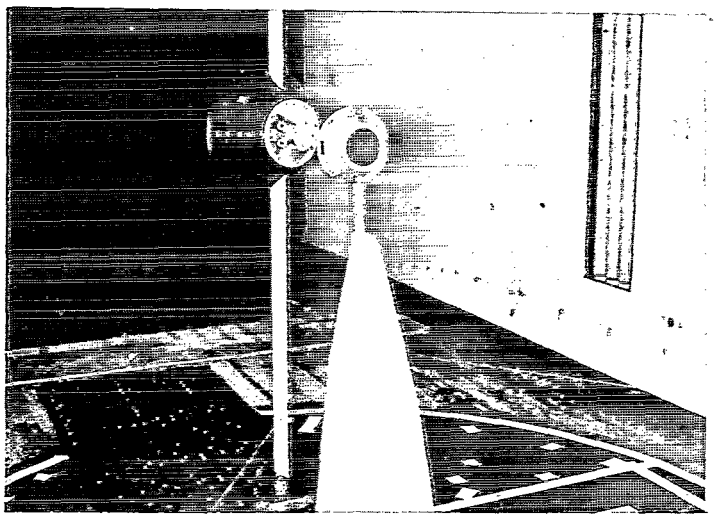

(c) Forward heat shield in wake of command module, single strut.

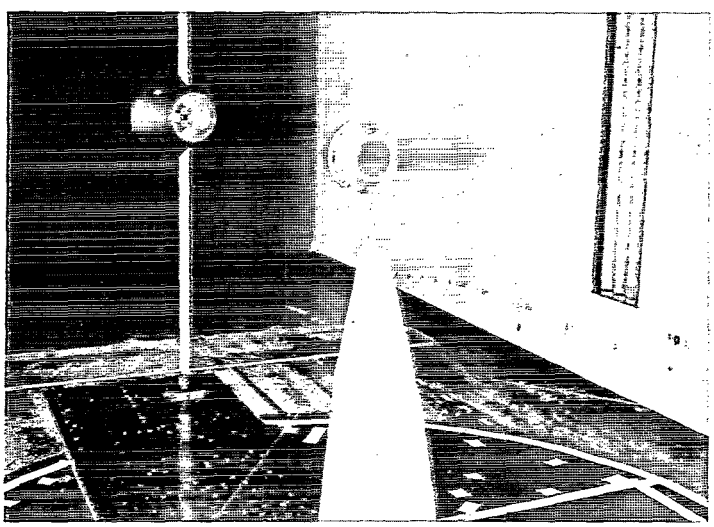

(d) Forward heat shield in wake of command module approximately 20 feet (full scale), single strut.

Figure 5. - Continued.

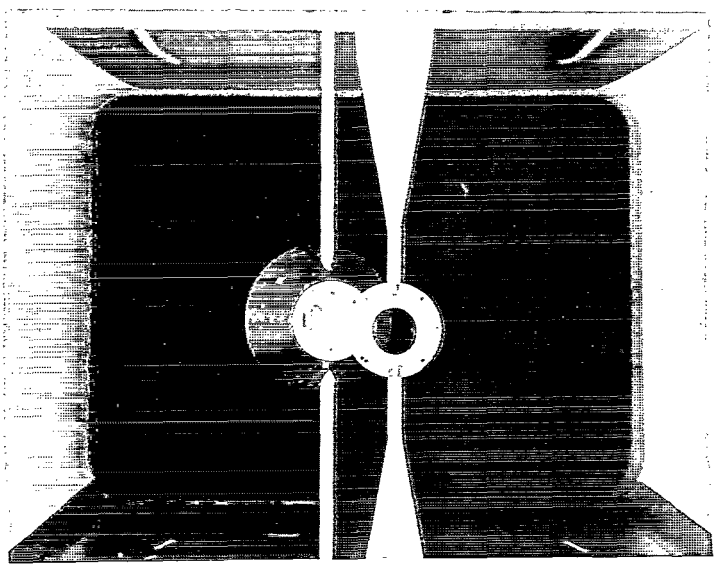

(e) Forward heat shield in wake of command module with image strut.

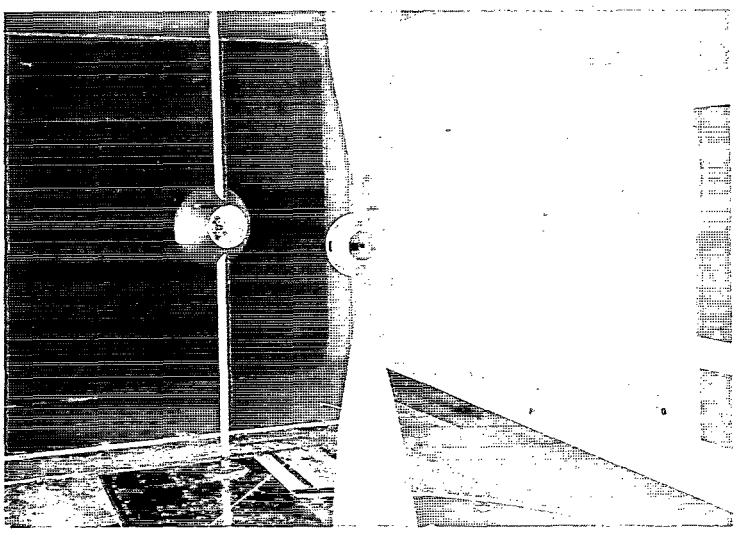

(f) Forward heat shield in wake of command module approximately 20 feet (full scale) with image strut.

Figure 5. - Concluded.

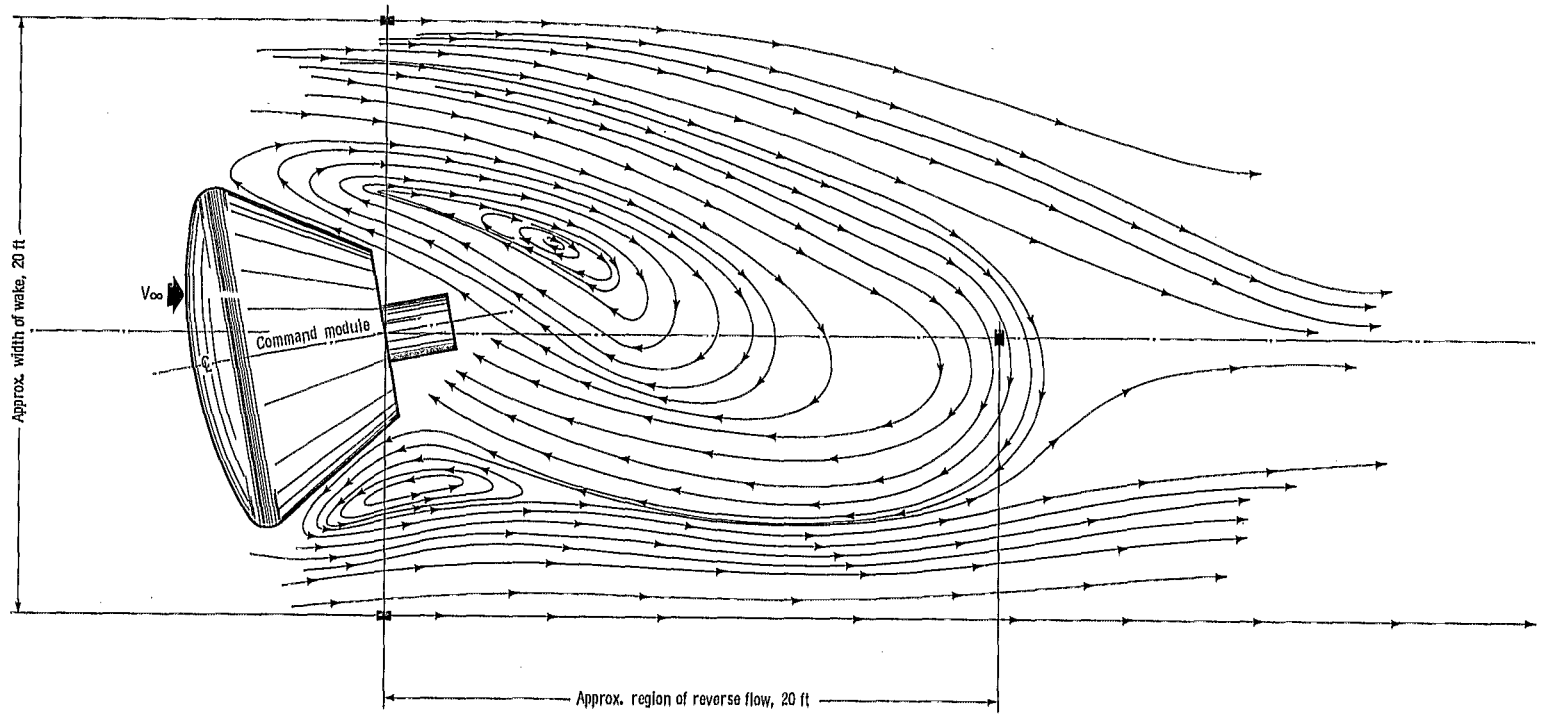

Figure 6. - Wake survey command module with a schematic of the velocity pattern.

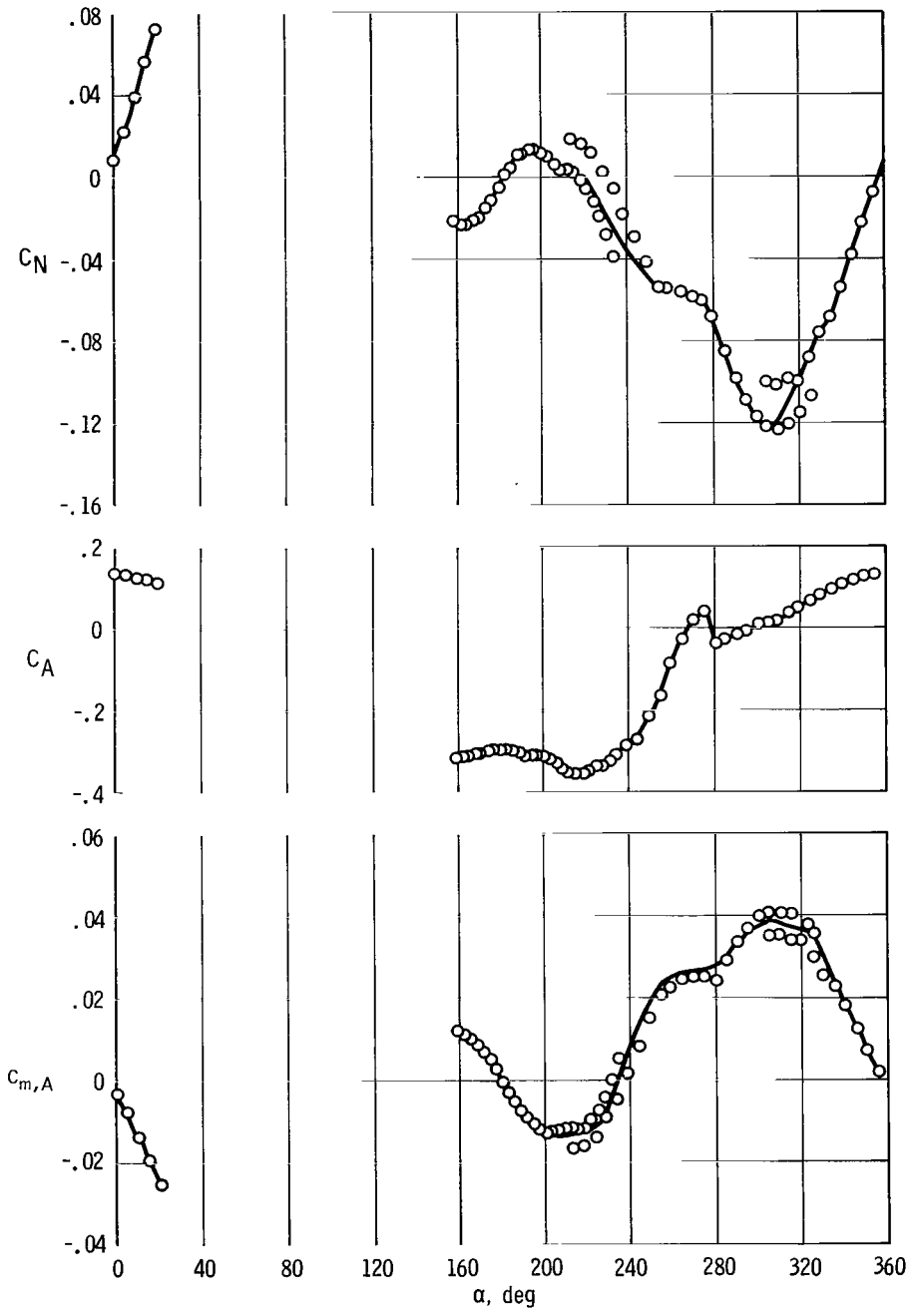

Figure 7. - Aerodynamic characteristics of the Block I forward heat shield (FHS) in free-stream flow.

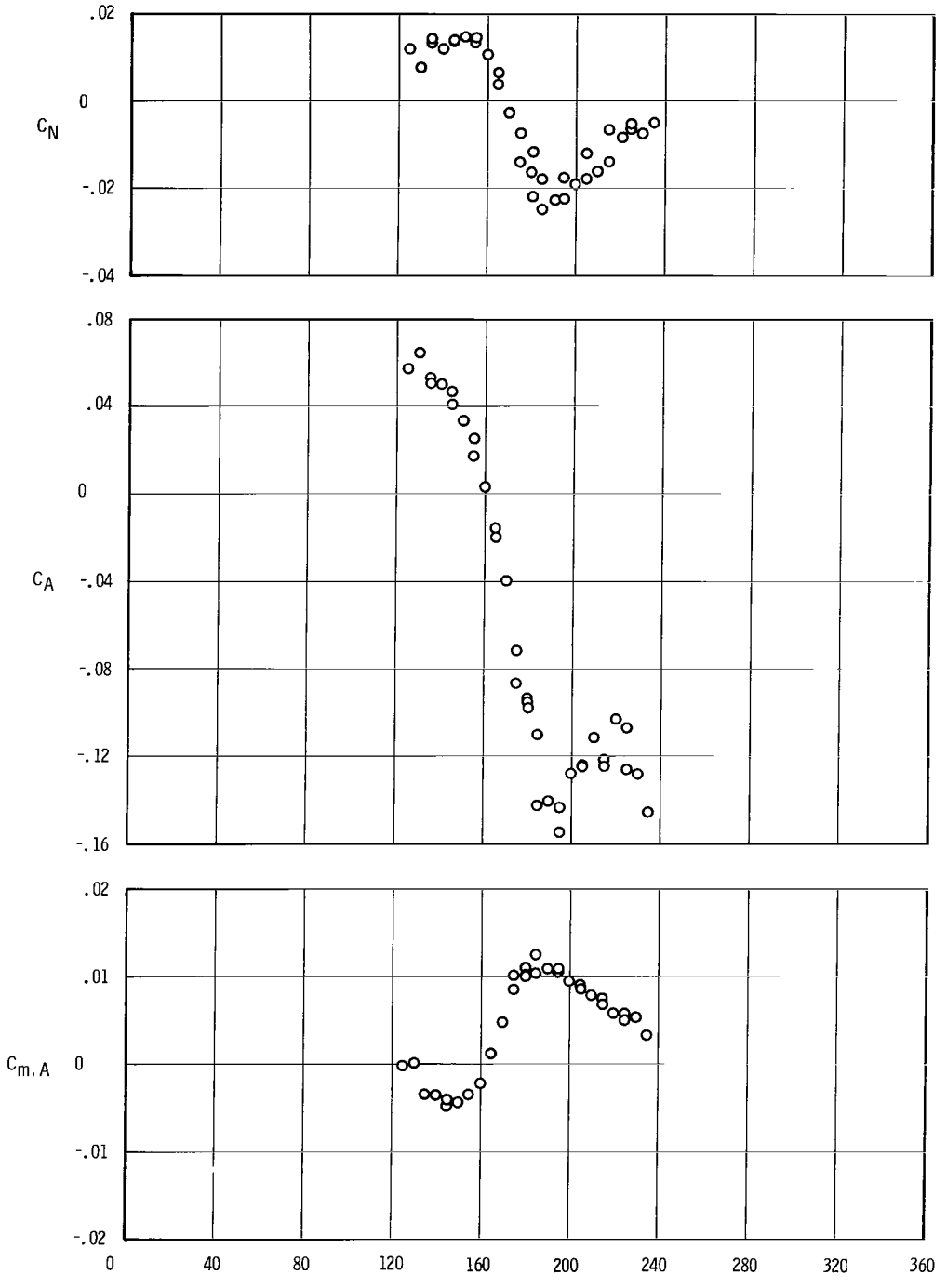

Figure 8. - Aerodynamic characteristics of the Block I forward heat shield (FHS) in the wake of the command module (X/D = 1.0, Z/D = 0.3).

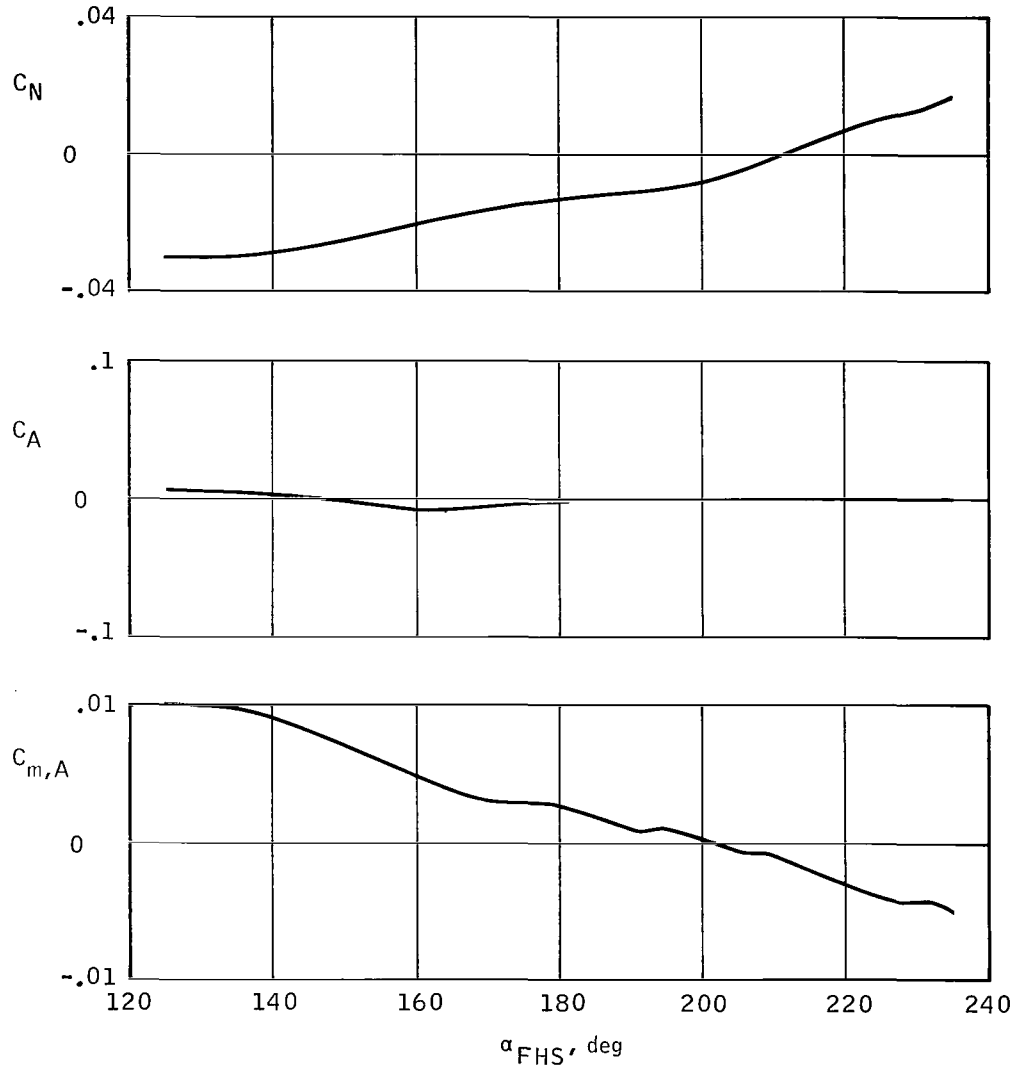

(a) X/D = 0.2, Z/D = 0.

Figure 9. - Aerodynamic characteristics of the Block I forward heat shield (FHS) in the wake of the command module.

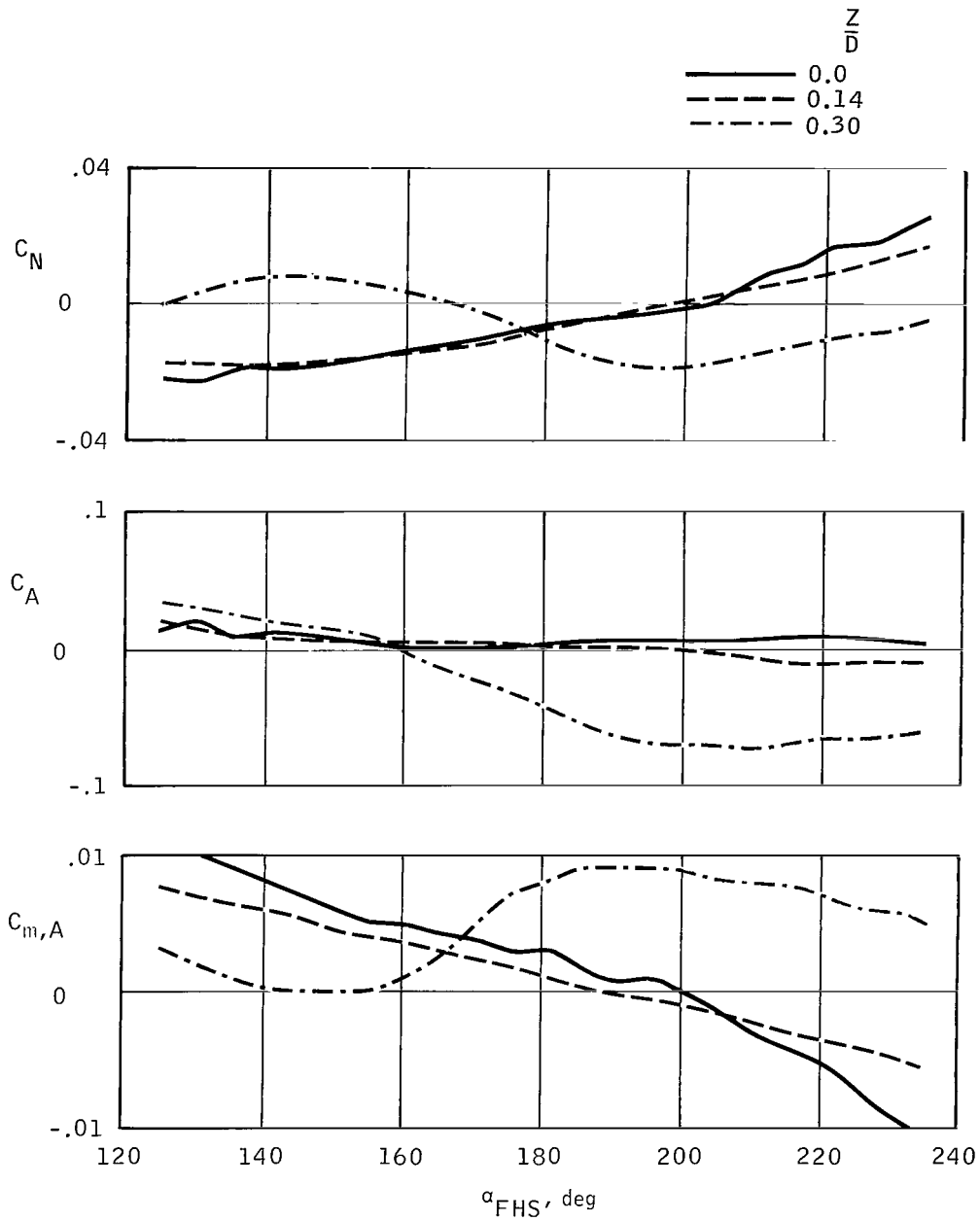

(b) X/D = 0.50.

Figure 9. - Continued.

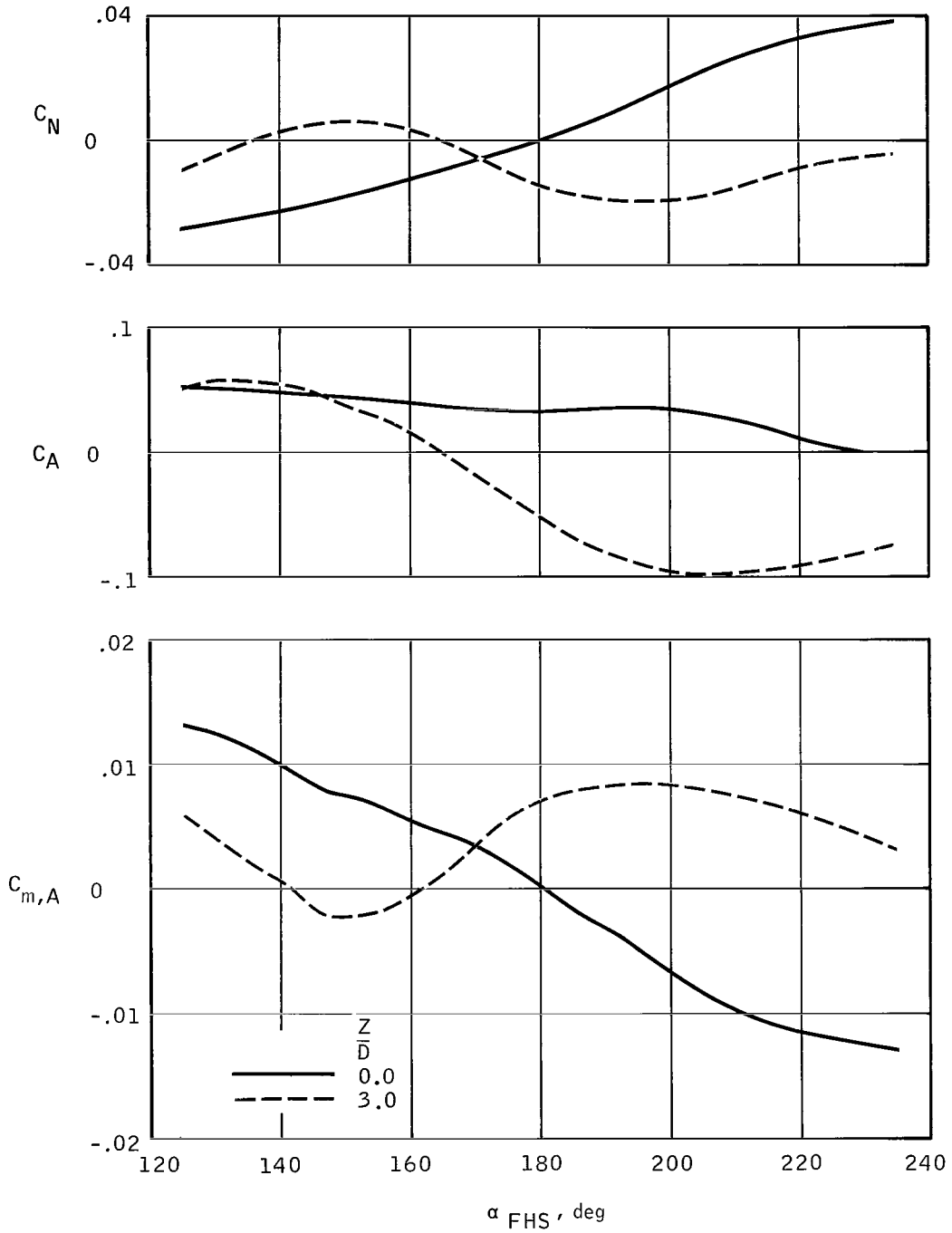

(c) X/D = 0.75.

Figure 9. - Continued.

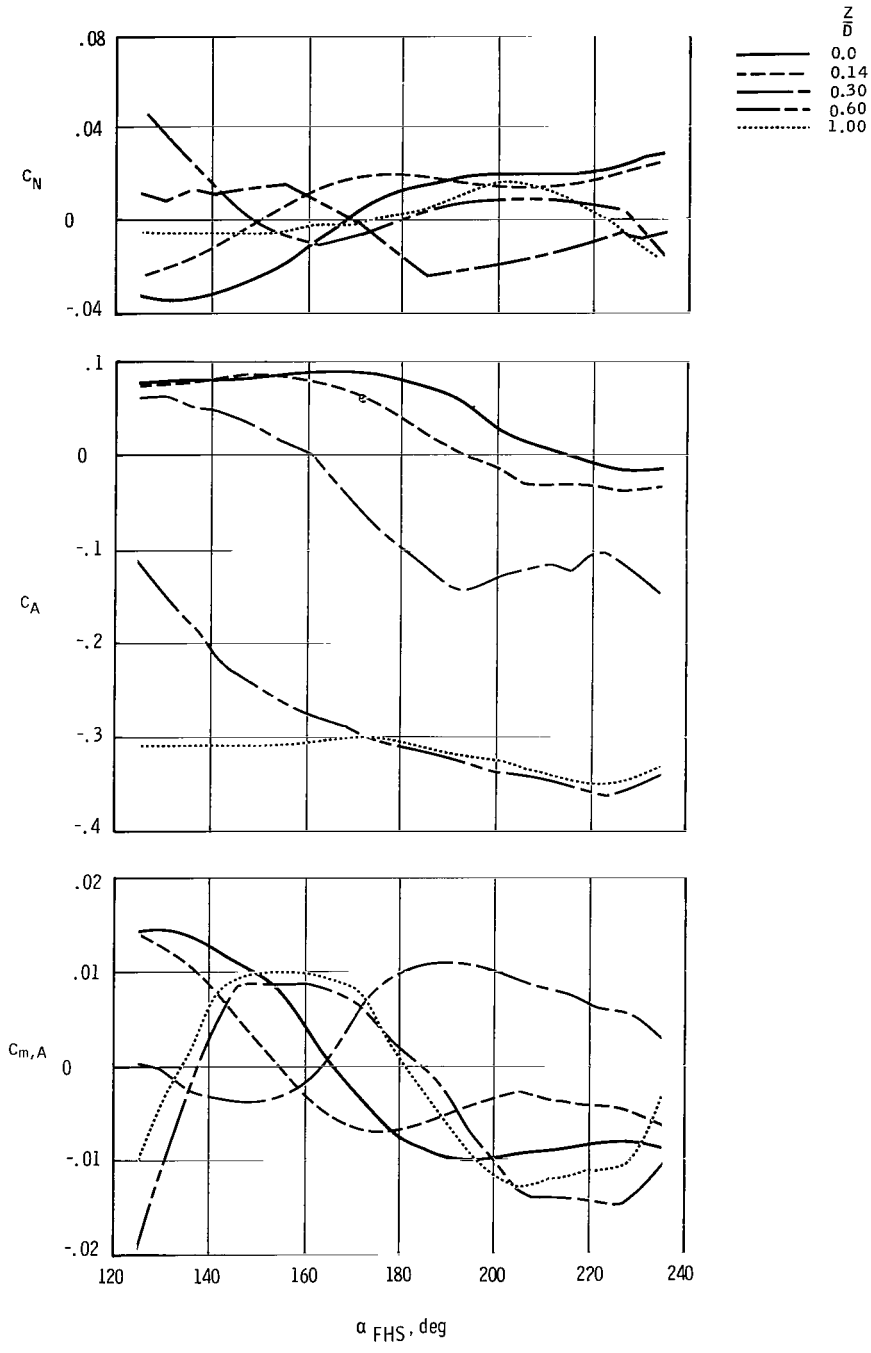

(d) X/D = 1.00.

Figure 9. - Continued.

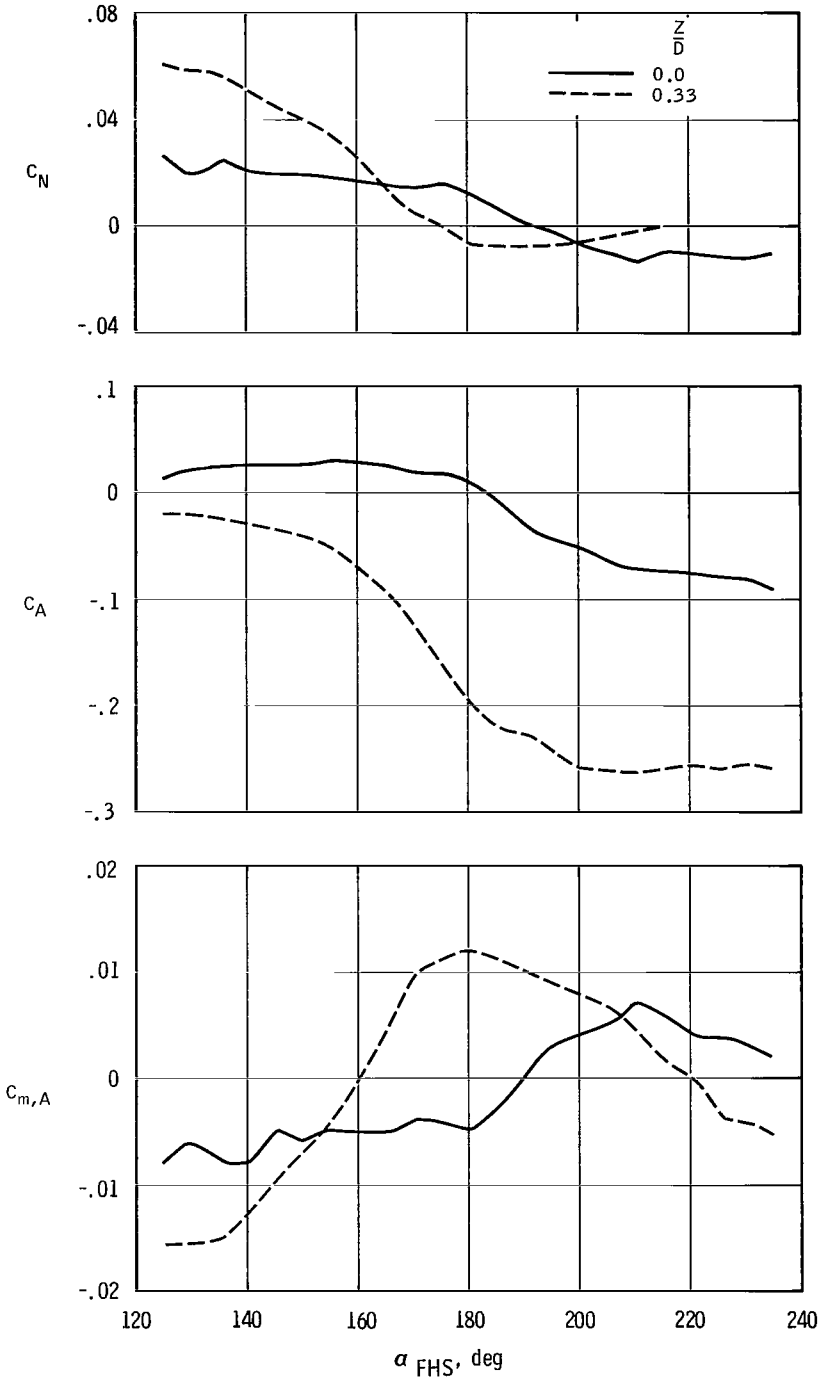

(e) X/D = 1.50.

Figure 9. - Continued.

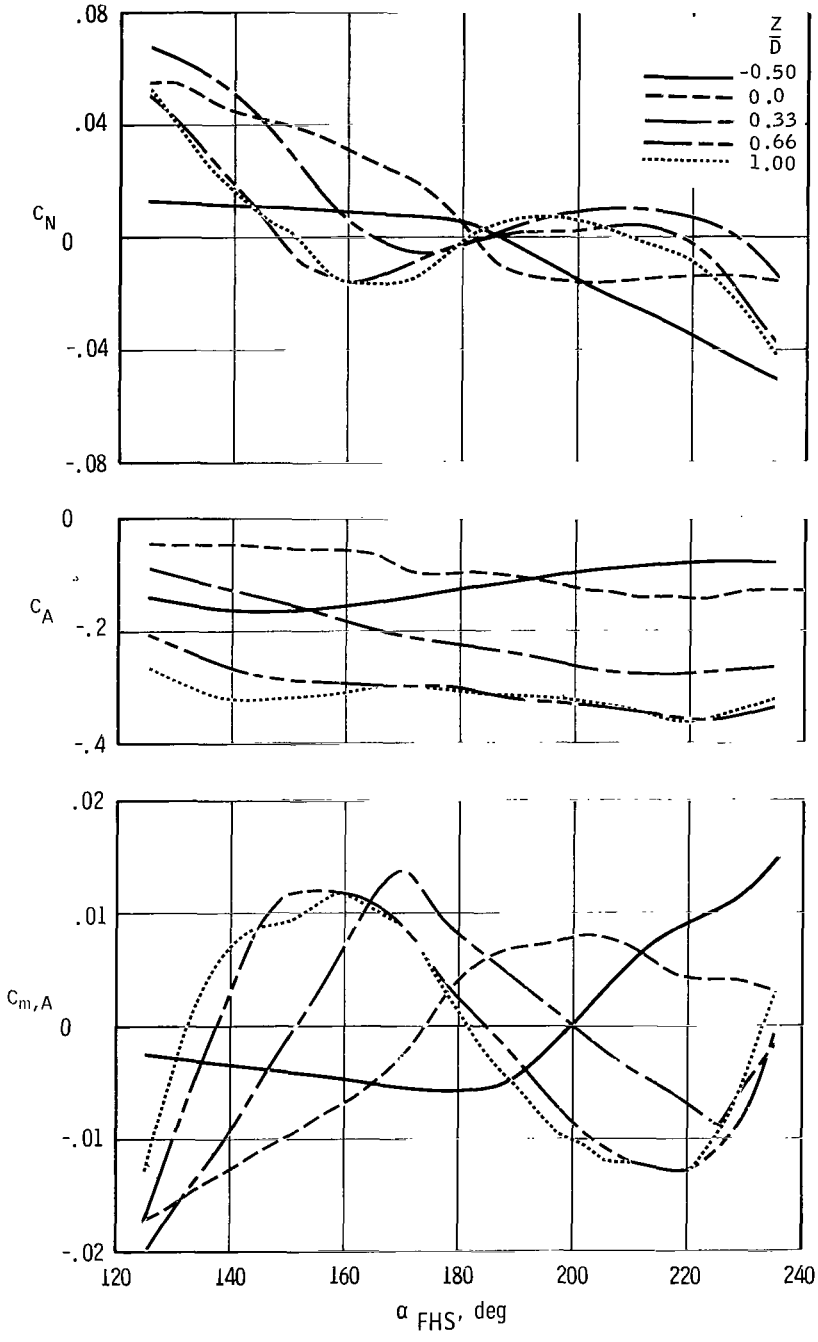

(f) X/D = 2.0.

Figure 9. - Continued.

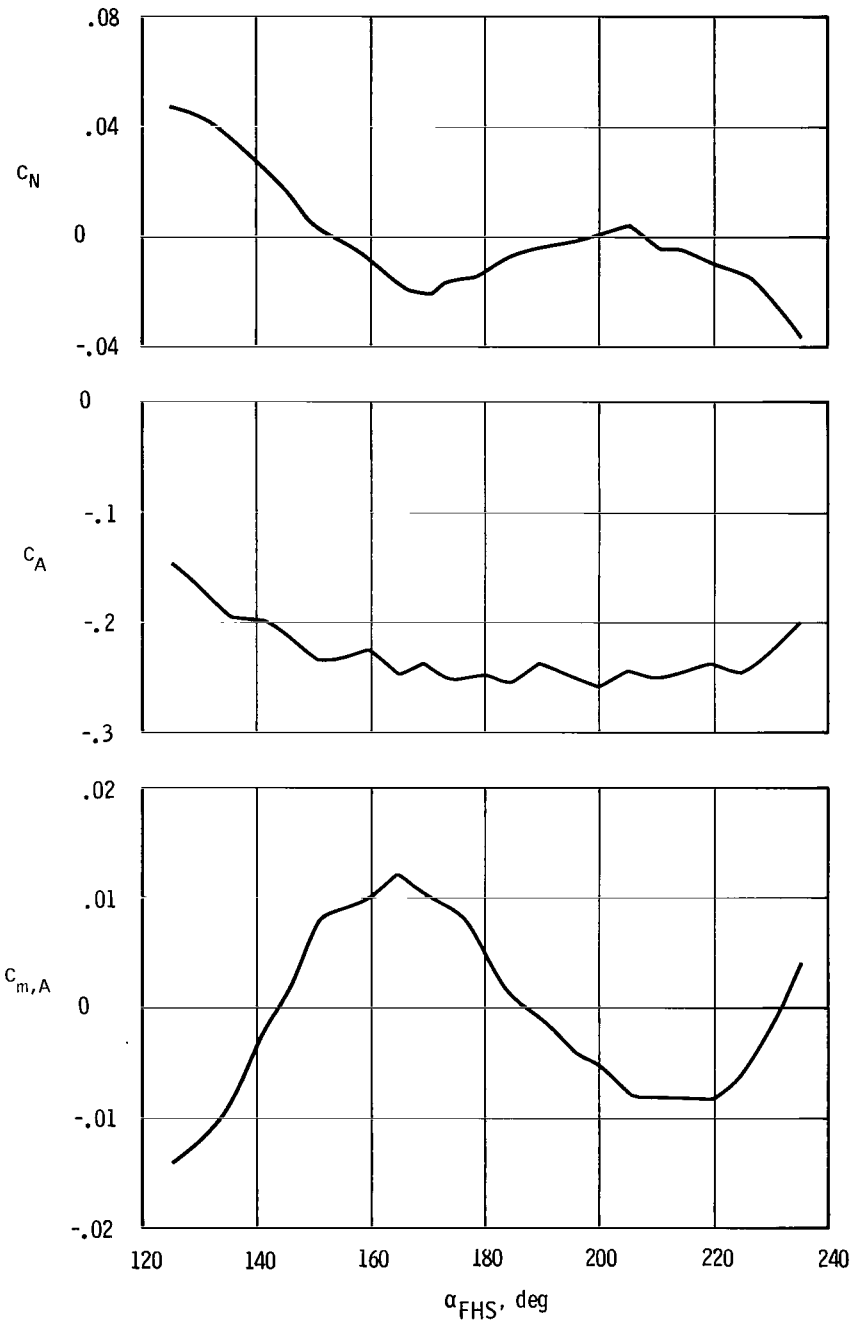

(g) X/D = 3.0, Z/D = 0.

Figure 9. - Concluded.

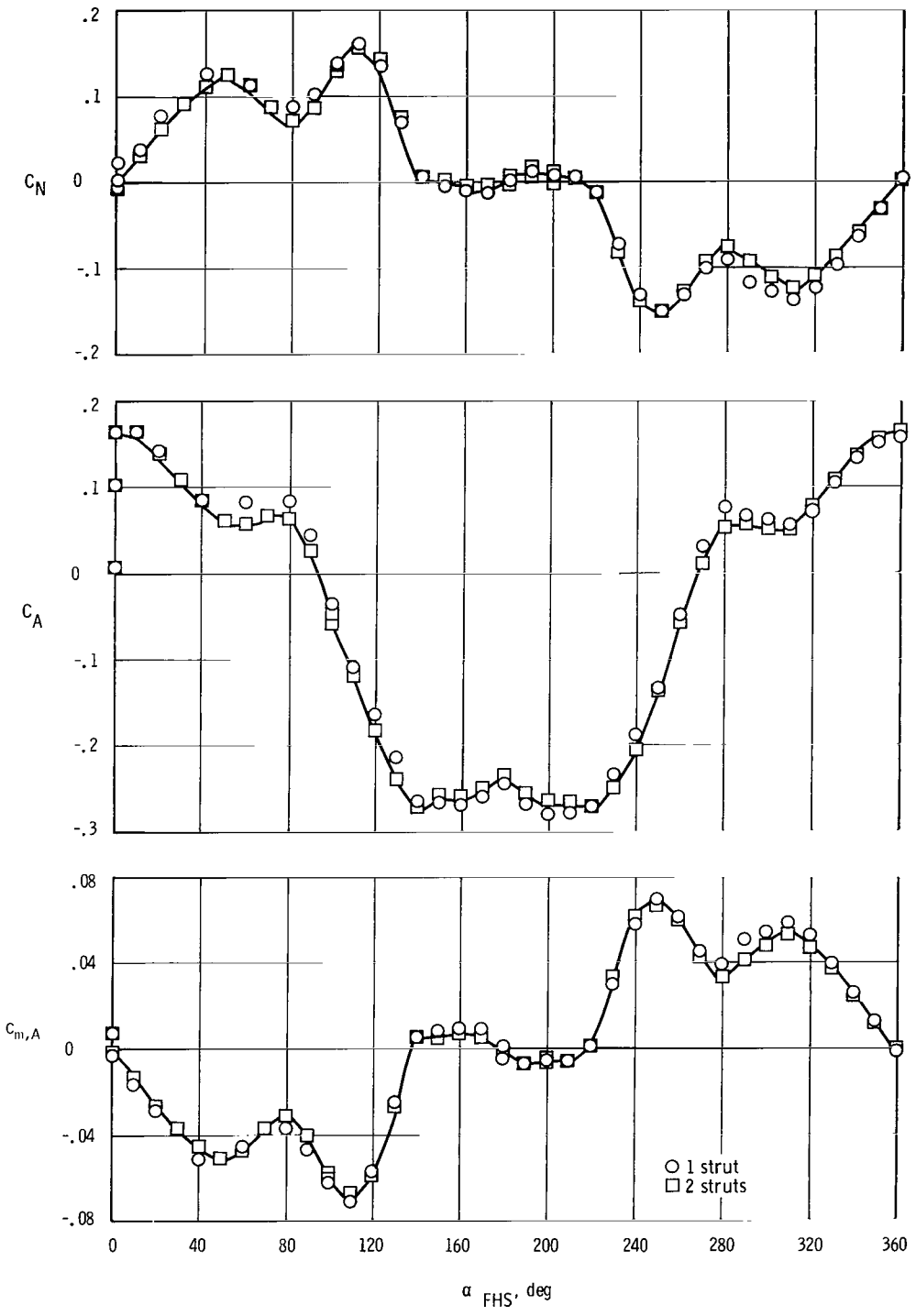

Figure 10. - Aerodynamic characteristics of the Block II forward heat shield (FHS) in free-stream flow (one strut and two struts).

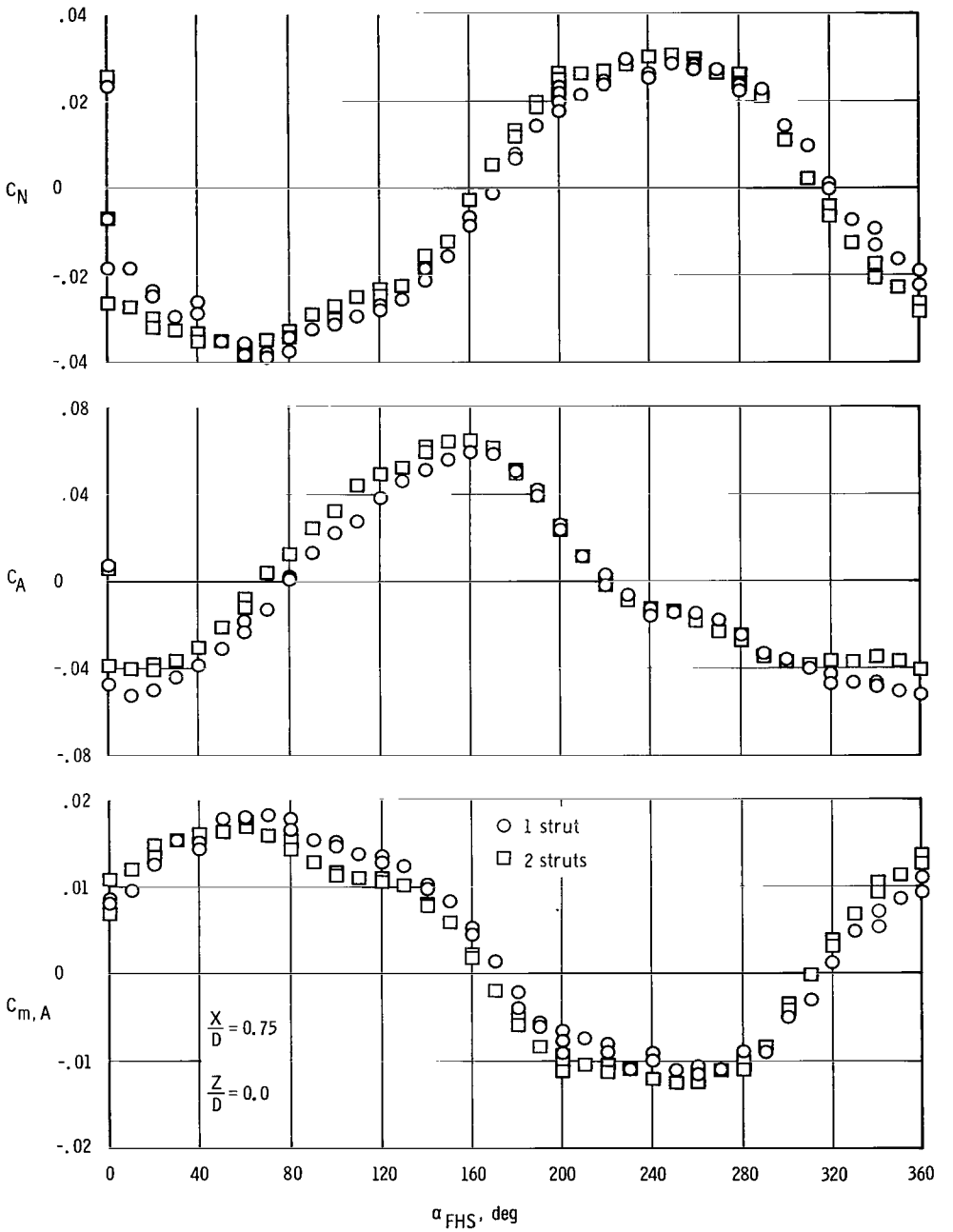

Figure 11. - Aerodynamic characteristics of the Block II forward heat shield (FHS) in the wake of the command module (one strut and two struts).

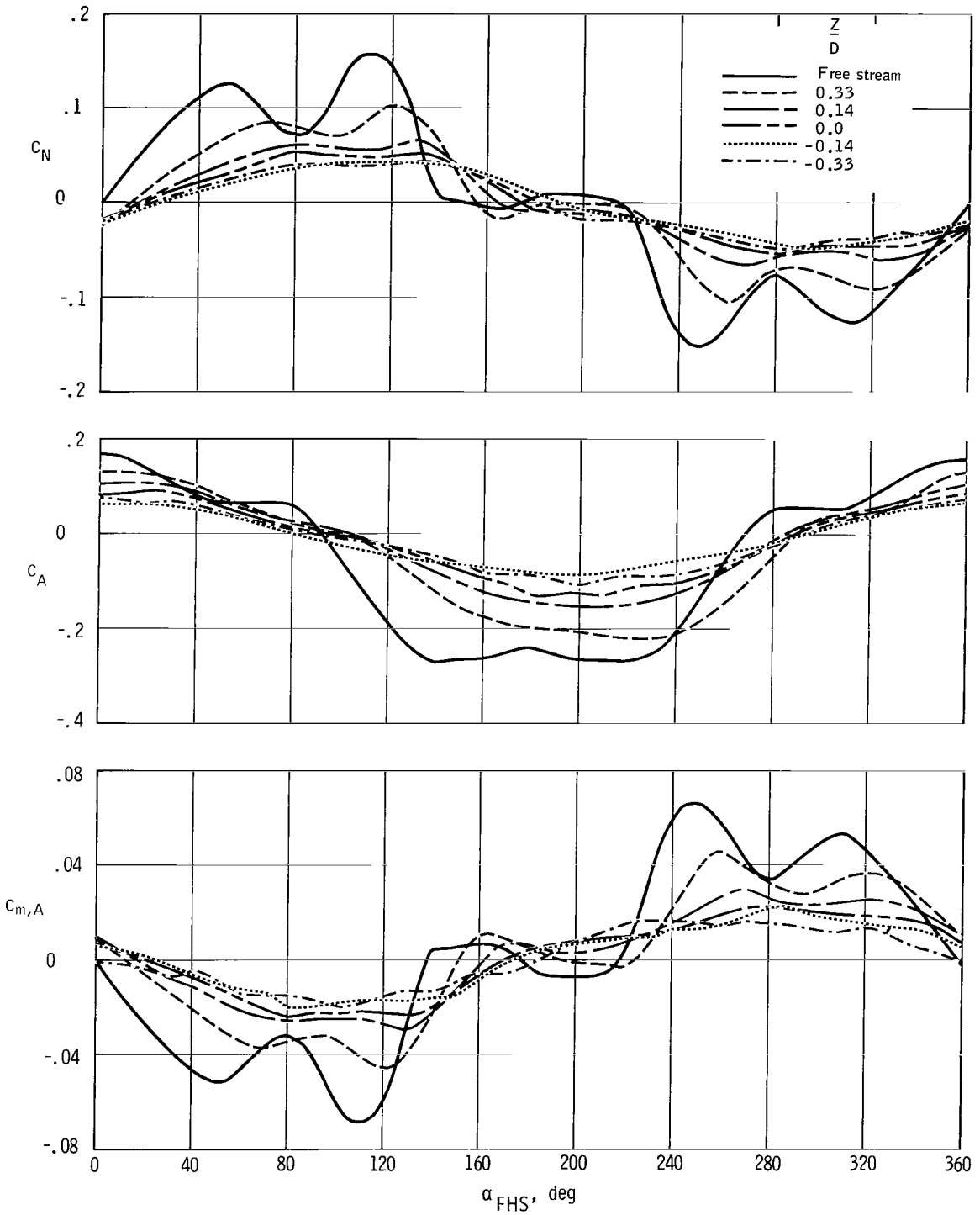

(a) X/D = 2.0.

Figure 12. - Aerodynamic characteristics of the Block II forward heat shield (FHS) in the wake of the command module and in free-stream flow (single strut).

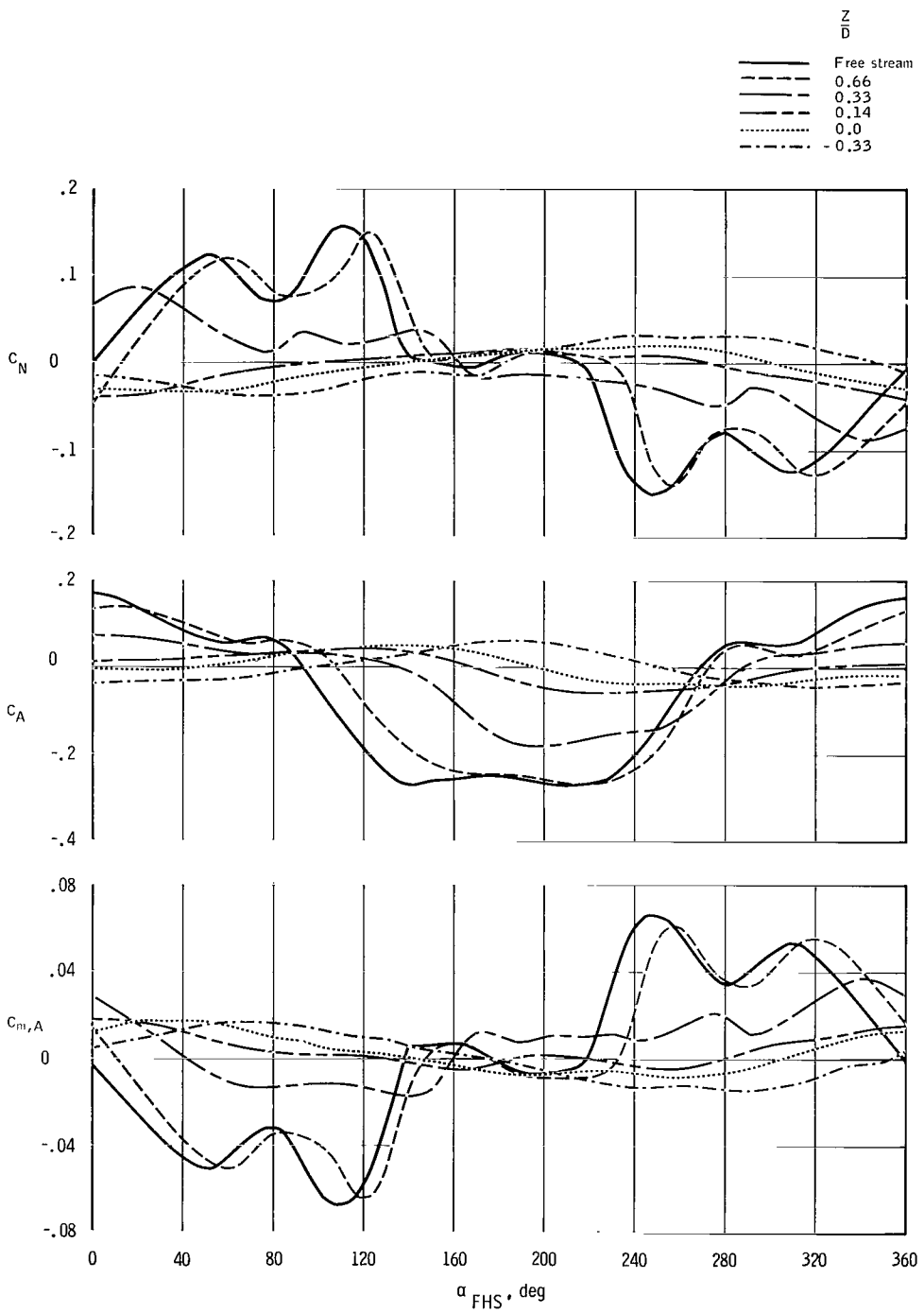

(b) X/D = 1.0.

Figure 12. - Continued.

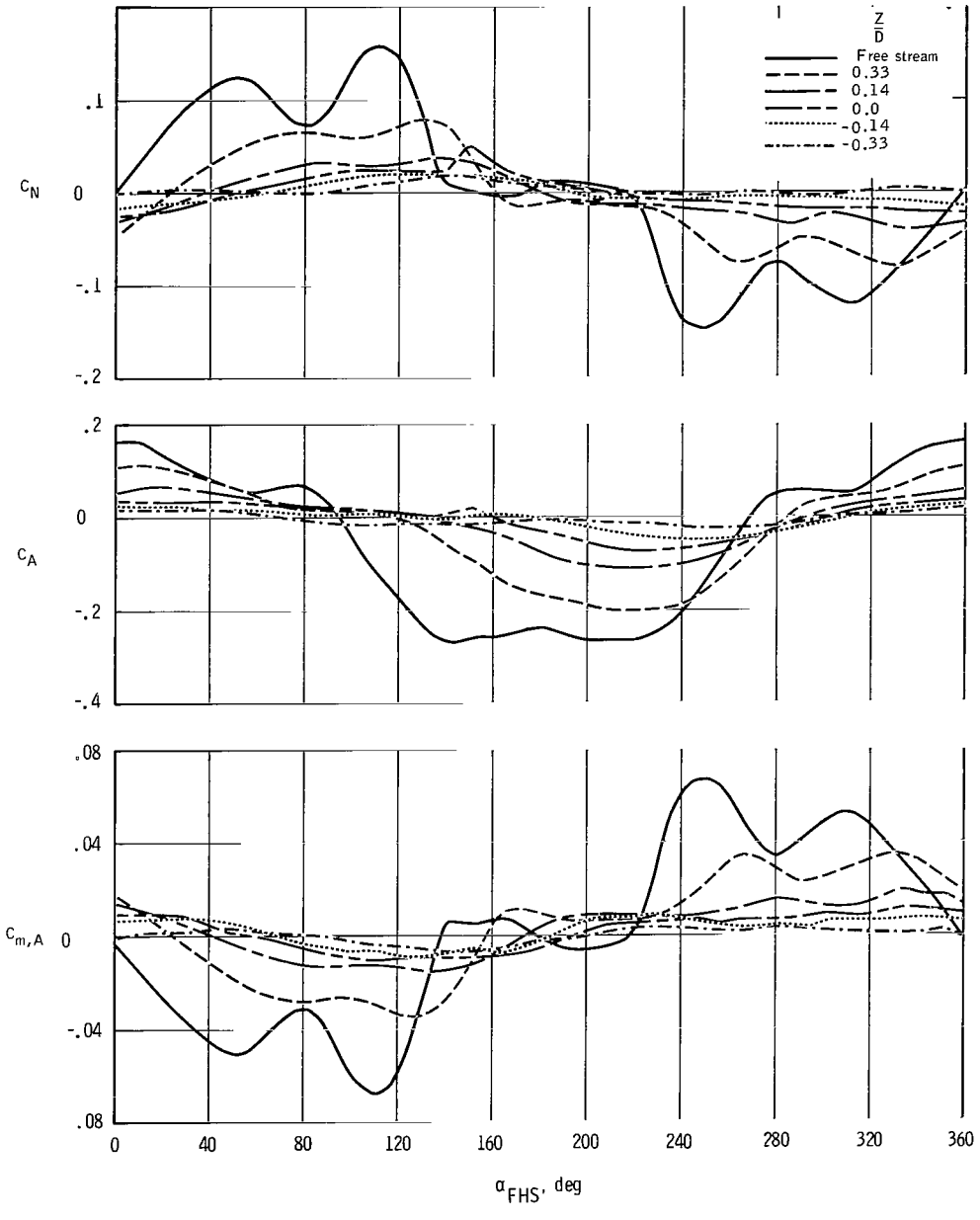

(c) X/D = 1.5.

Figure 12. - Continued.

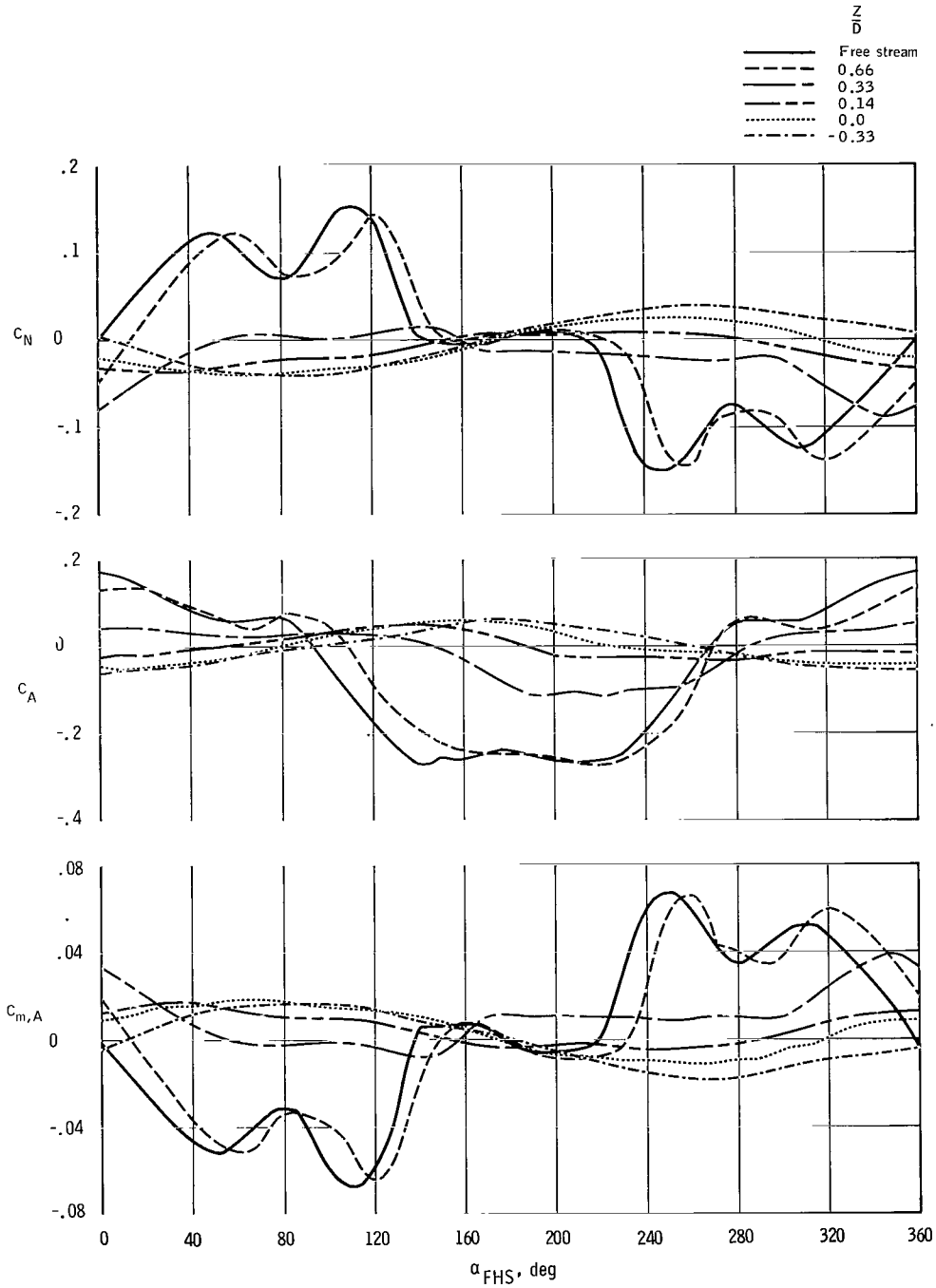

(d) X/D = 0.75.

Figure 12. - Continued.

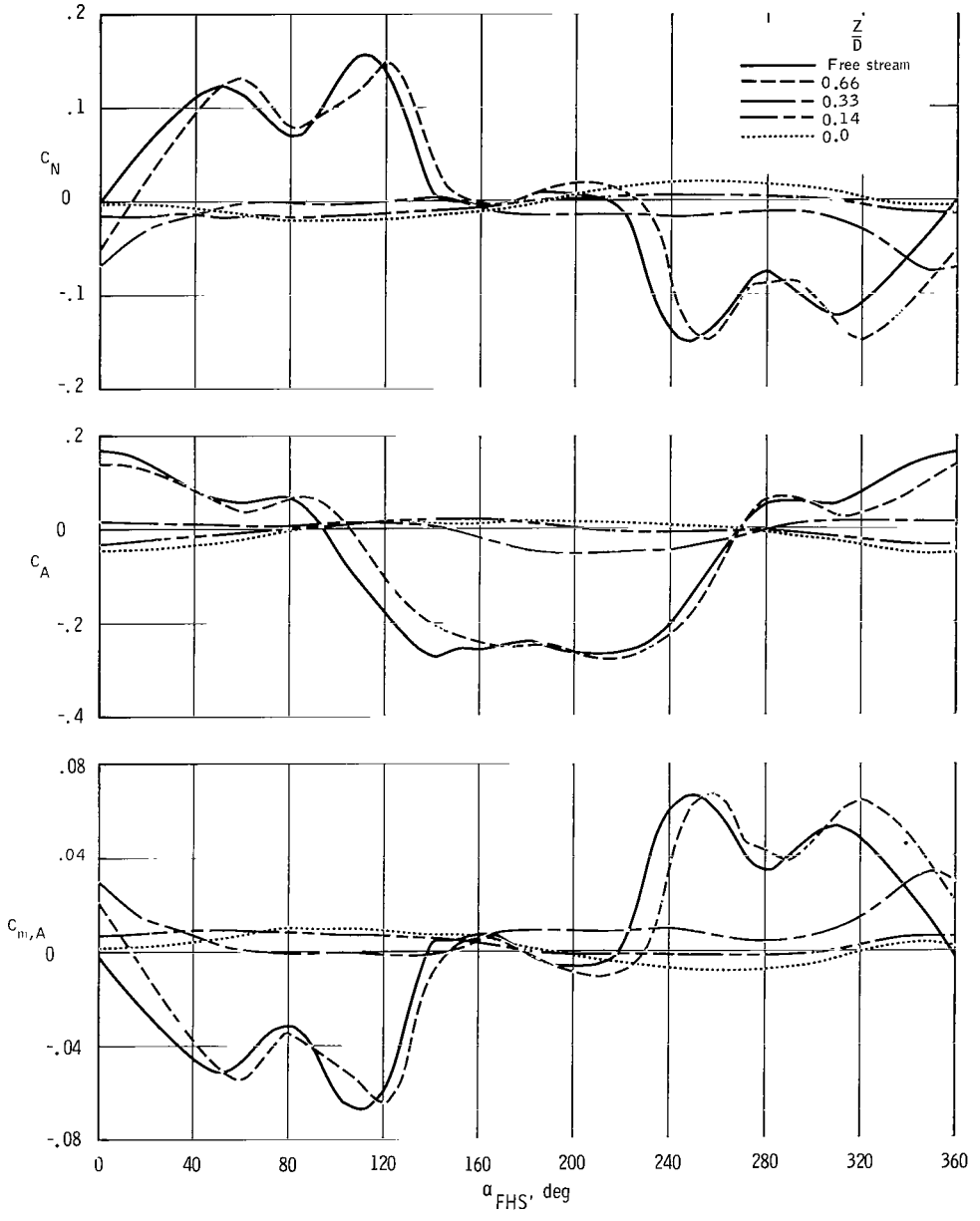

(e) X/D = 0.5.

Figure 12. - Continued.

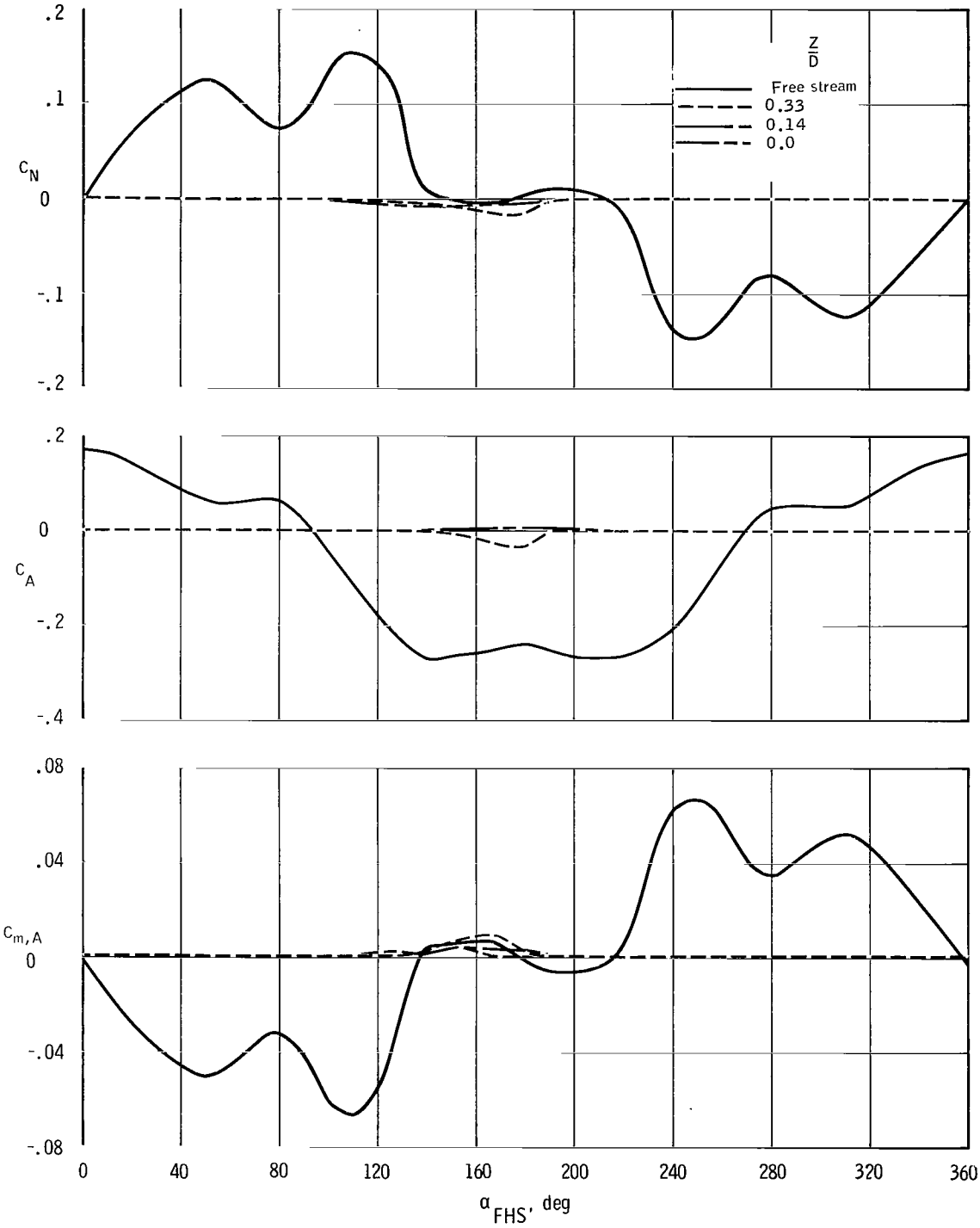

(f) X/D = 0.20.

Figure 12. - Continued.

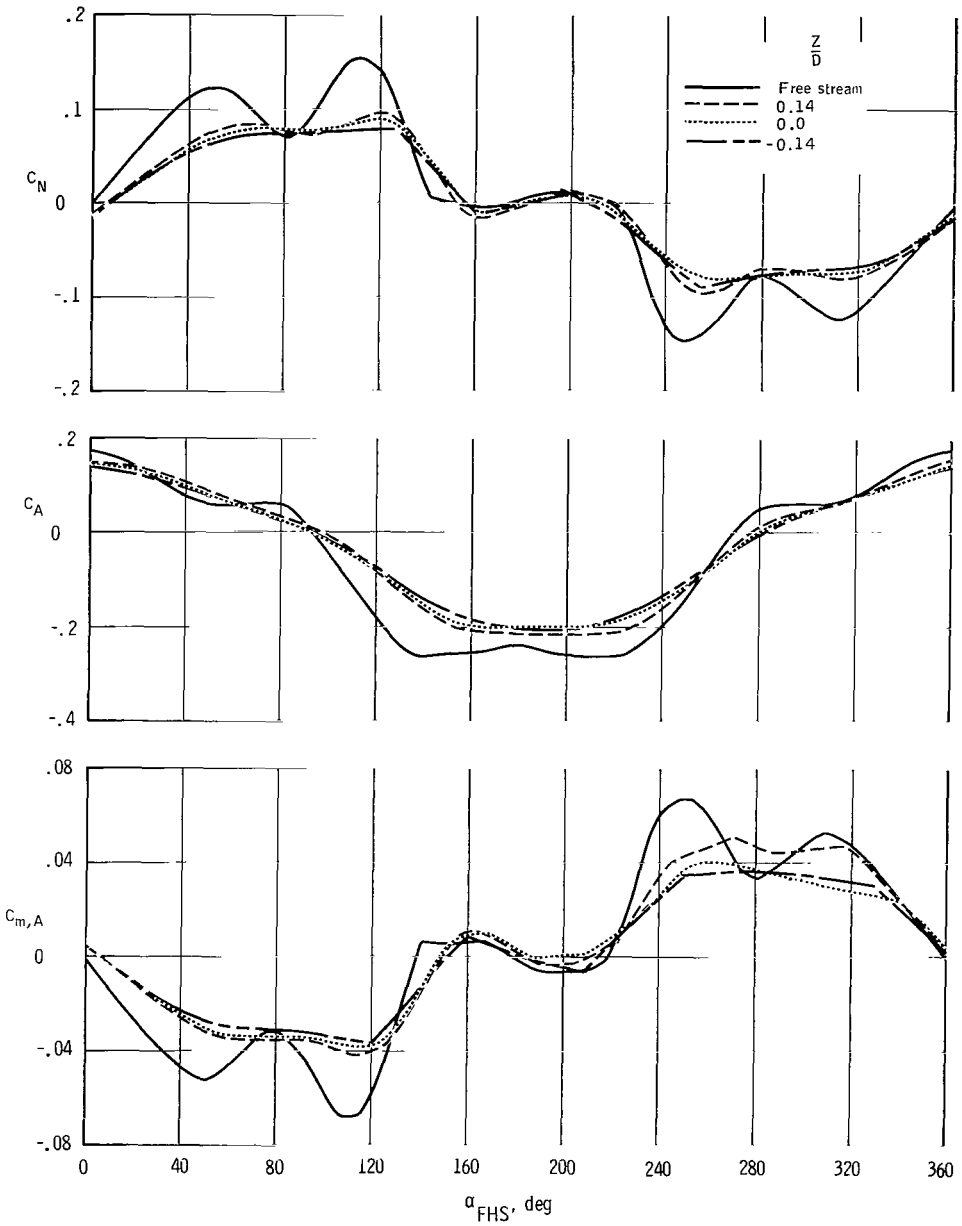

(g) X/D = 3.0.

Figure 12. - Continued.

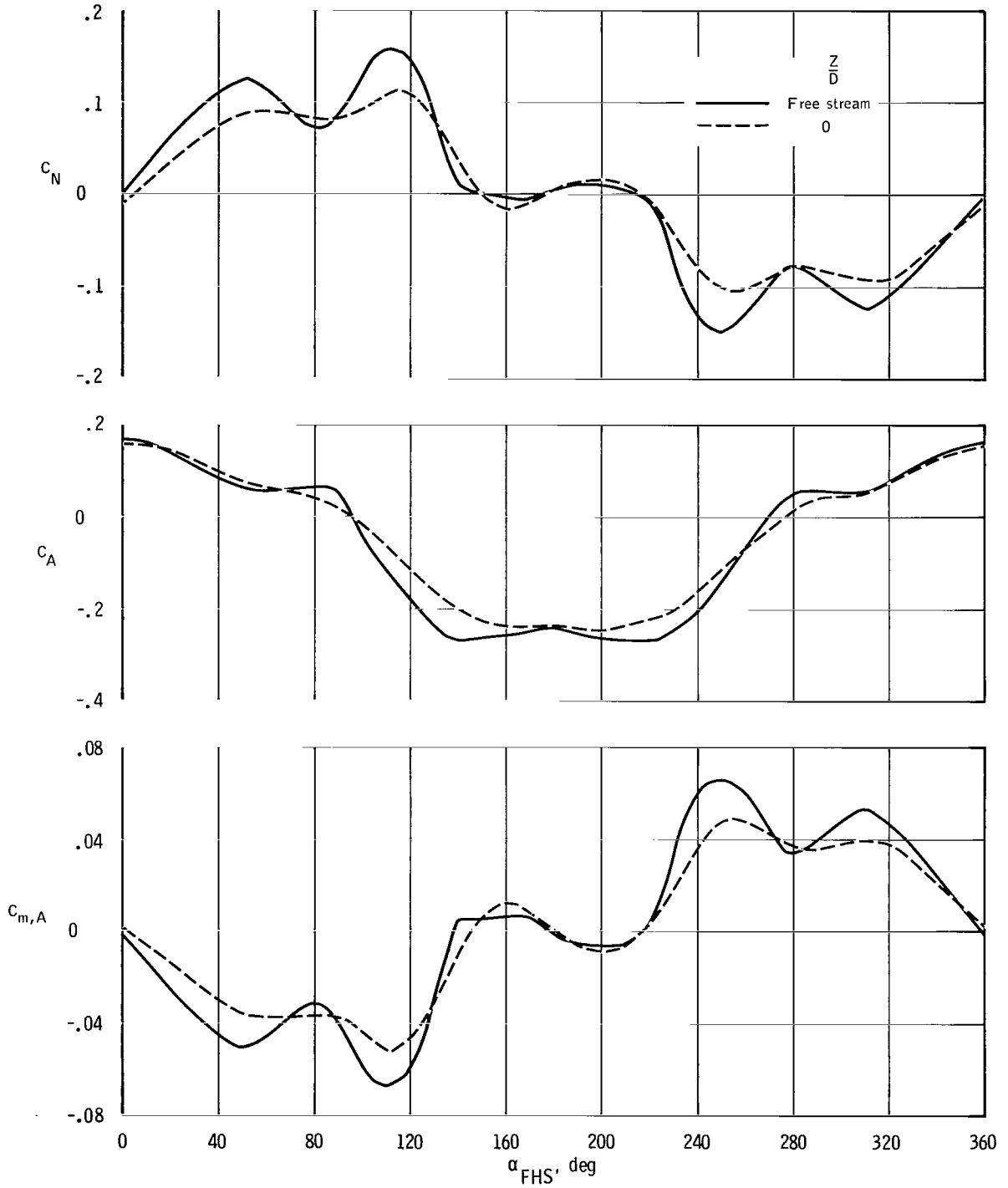

(h) X/D = 4.0.

Figure 12. - Concluded.

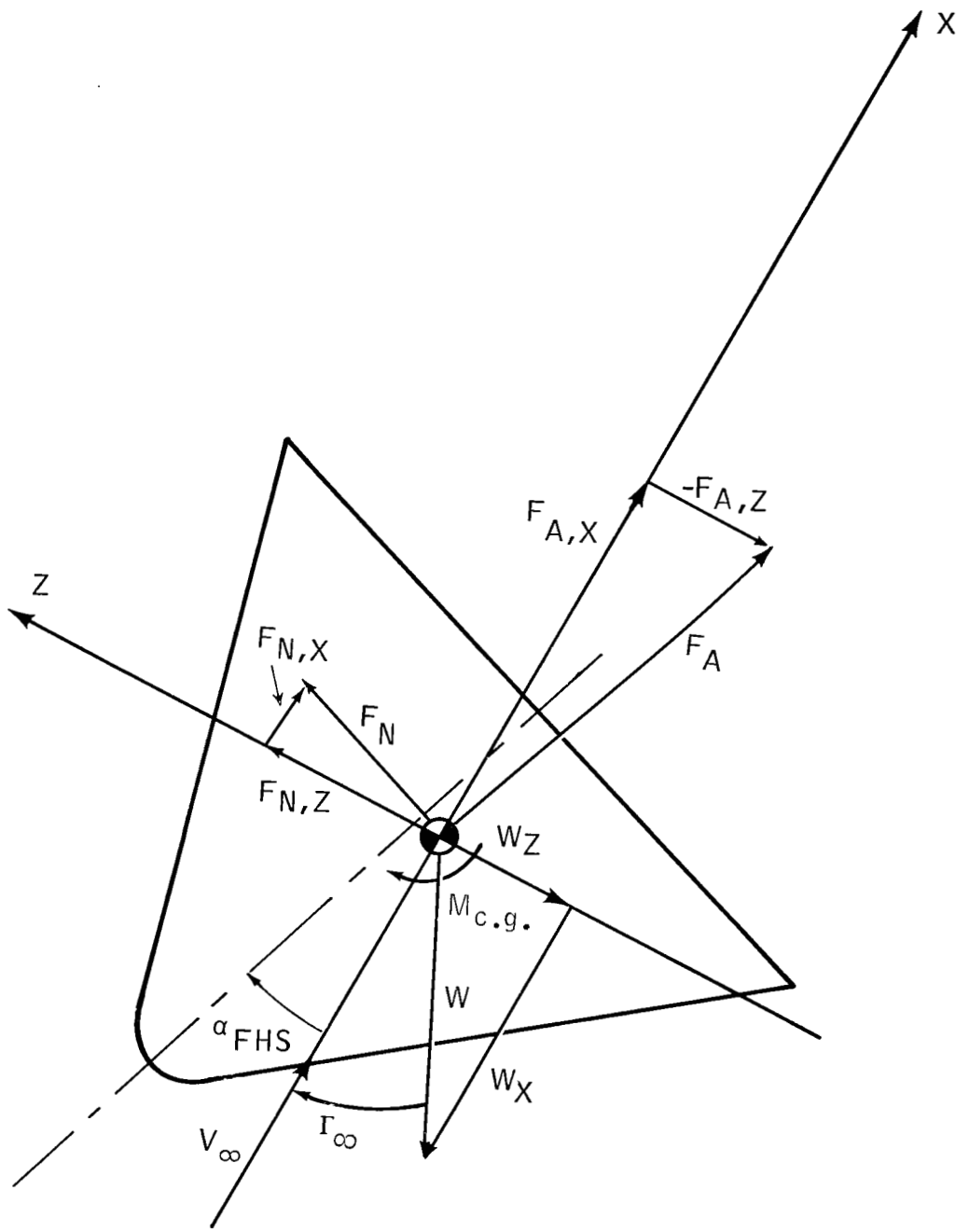

Figure 13. - Free-body diagram of forward heat shield (FHS).

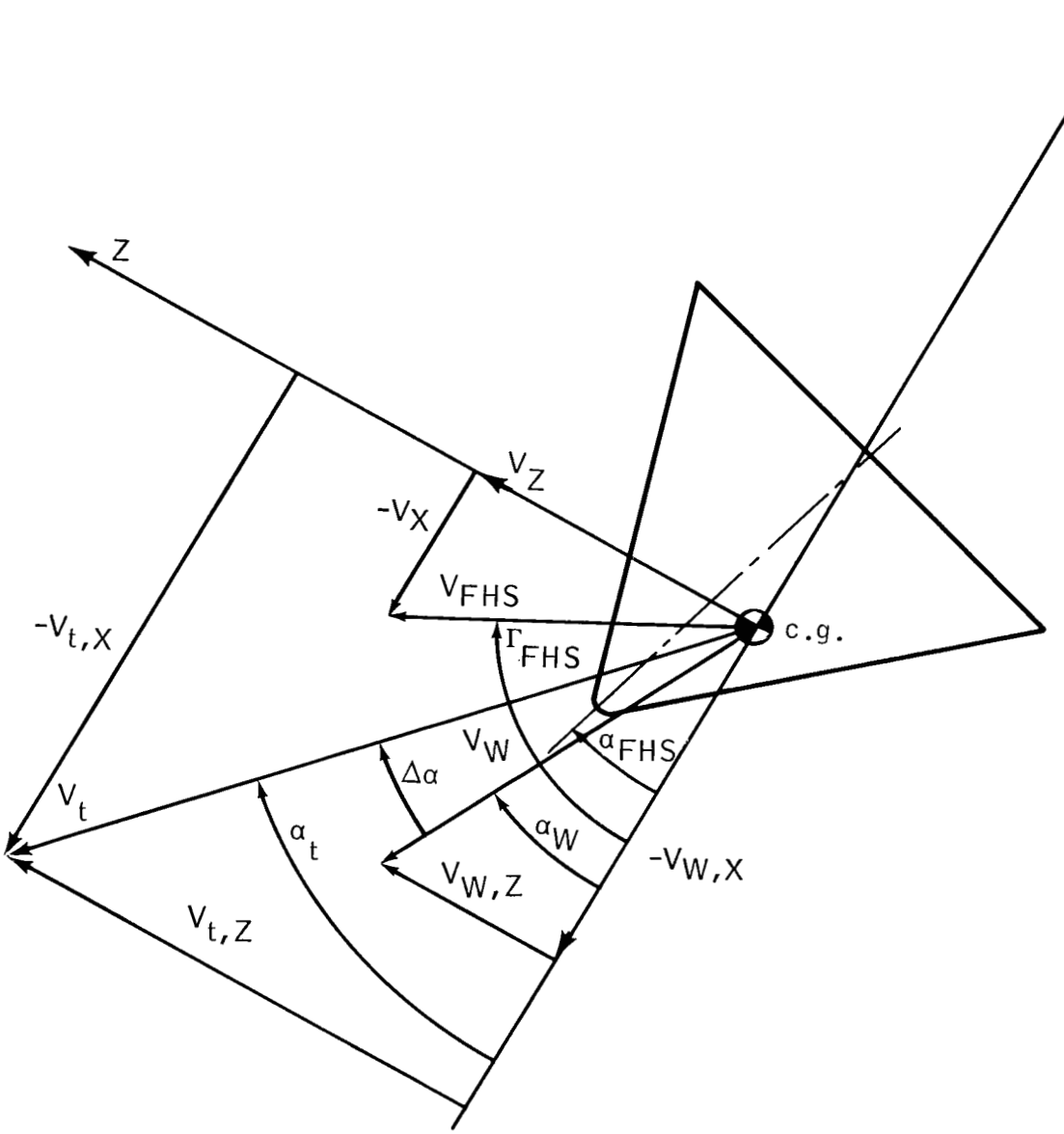

Figure 14. - Forward heat-shield (FHS) velocity vectors.

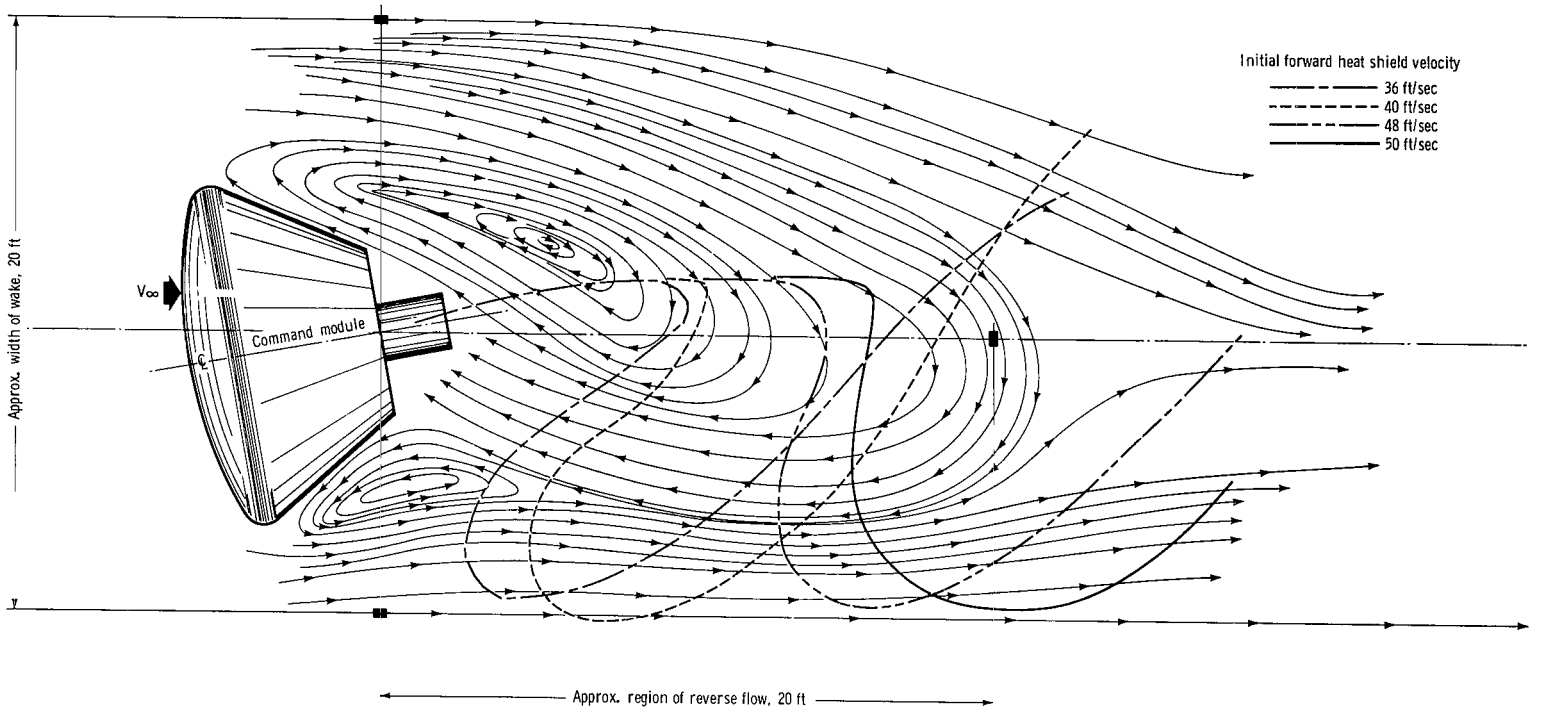

Figure 15. - Block I forward heat-shield center-of-gravity trajectories in wake of command module.

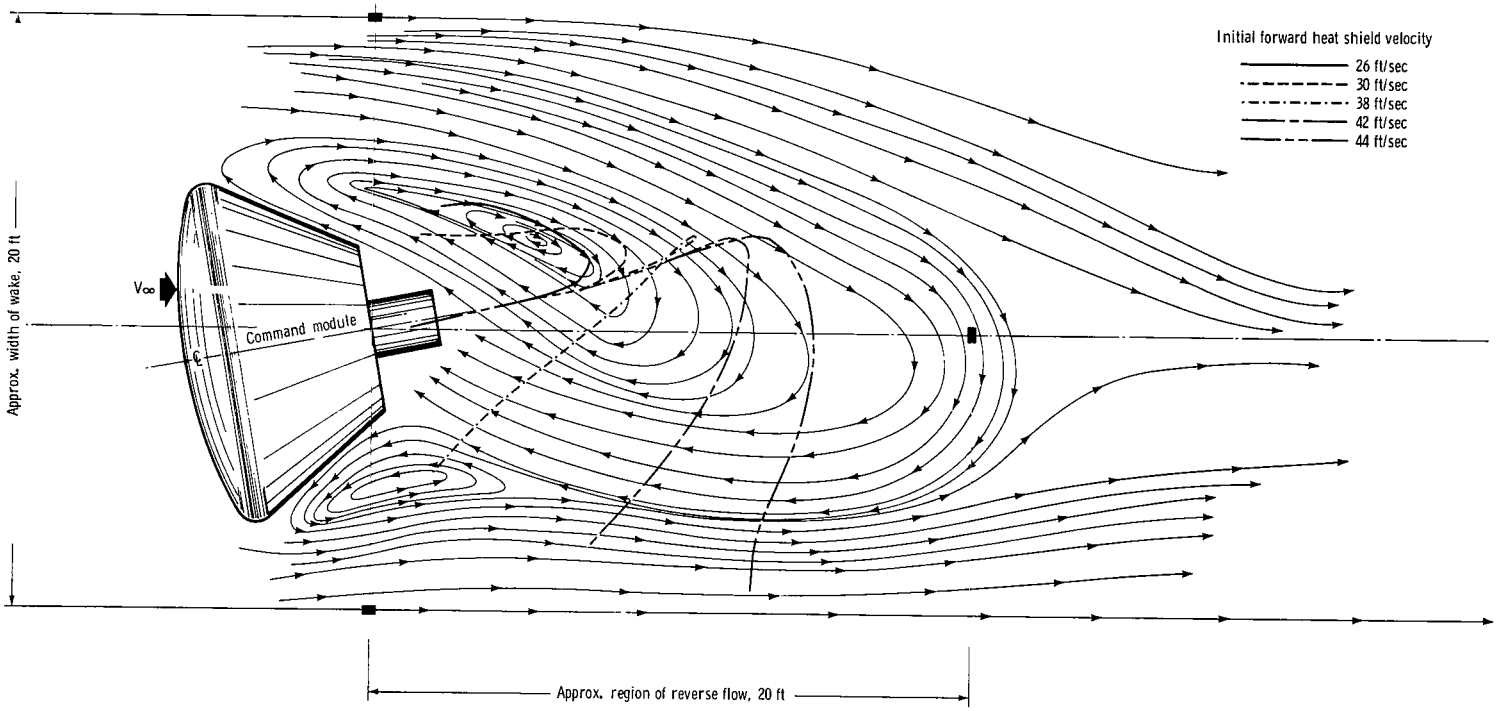

Figure 16. - Block II forward heat-shield center-of-gravity trajectories in wake of command module.

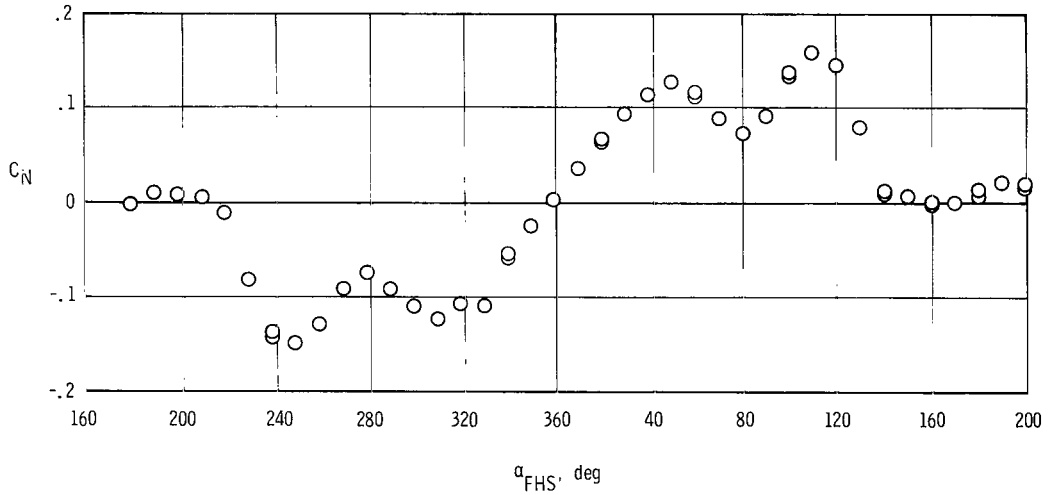

(a) FHS in free stream, one strut.

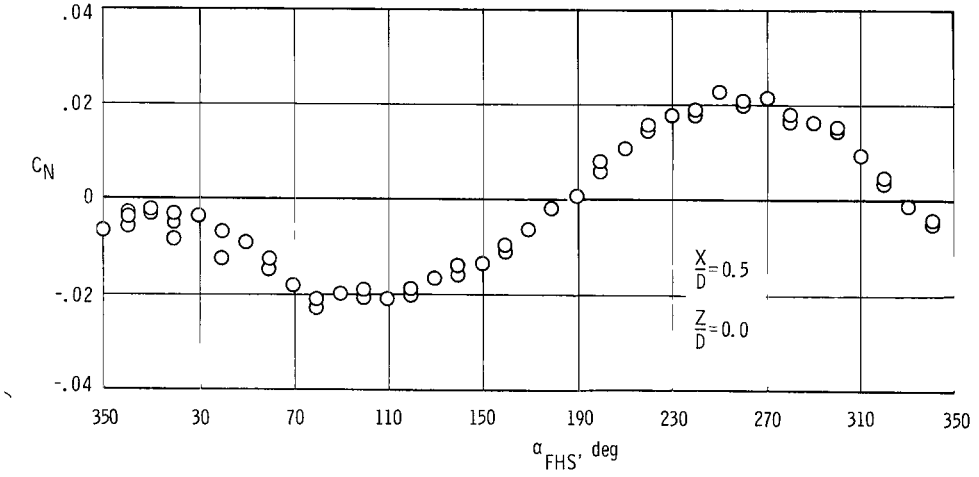

(b) FHS in one strut.

Figure 17. - Arbitrary aerodynamic plot compared to a free-stream plot.

NATIONAL AERONAUTICS AND SPACE ADMINISTRATION
WASHINGTON, D. C. 20546

OFFICIAL BUSINESS

FIRST CLASS MAIL

POSTAGE AND FEES PAID
NATIONAL AERONAUTICS AND
SPACE ADMINISTRATION

"The aeronautical and space activities of the United States shall be conducted so as to contribute . . . to the expansion of human knowledge of phenomena in the atmosphere and space. The Administration shall provide for the widest practicable and appropriate dissemination of information concerning its activities and the results thereof."

—NATIONAL AERONAUTICS AND SPACE ACT OF 1958

NASA SCIENTIFIC AND TECHNICAL PUBLICATIONS

TECHNICAL REPORTS: Scientific and technical information considered important, complete, and a lasting contribution to existing knowledge.

TECHNICAL NOTES: Information less broad in scope but nevertheless of importance as a contribution to existing knowledge.

TECHNICAL MEMORANDUMS: Information receiving limited distribution because of preliminary data, security classification, or other reasons.

CONTRACTOR REPORTS: Scientific and technical information generated under a NASA contract or grant and considered an important contribution to existing knowledge.

TECHNICAL TRANSLATIONS: Information published in a foreign language considered to merit NASA distribution in English.

SPECIAL PUBLICATIONS: Information derived from or of value to NASA activities. Publications include conference proceedings, monographs, data compilations, handbooks, sourcebooks, and special bibliographies.

TECHNOLOGY UTILIZATION PUBLICATIONS: Information on technology used by NASA that may be of particular interest in commercial and other non-aerospace applications. Publications include Tech Briefs, Technology Utilization Reports and Notes, and Technology Surveys.

Details on the availability of these publications may be obtained from:

SCIENTIFIC AND TECHNICAL INFORMATION DIVISION

NATIONAL AERONAUTICS AND SPACE ADMINISTRATION

Washington, D.C. 20546